Numerical investigation of heat transfer in a CO_2 two-phase ejector

Michal Haida[a,*], Jacek Smolka[a], Armin Hafner[b], Mikolaj Mastrowski[a], Michał Palacz[a], Kenneth B. Madsen[c], Andrzej J. Nowak[a], Krzysztof Banasiak[d]

[a]*Institute of Thermal Technology, Silesian University of Technology, Konarskiego 22, 44-100 Gliwice, Poland*
[b]*NTNU Department of Energy and Process Engineering, Kolbjørn Hejes vei 1d, 7465 Trondheim, Norway*
[c]*Danfoss Company, Denmark*
[d]*SINTEF Energy, Kolbjørn Hejes vei 1d, 7465 Trondheim, Norway*

Abstract

In this paper, the influence of heat transfer in the walls of an R744 two-phase ejector on ejector performance was investigated. A numerical investigation was performed using a computational fluid dynamic (CFD) model of the R744 two-phase flow coupled with the heat transfer inside the ejector. An ejector equipped with thermocouple channels was designed and manufactured to investigate temperature distribution in the inner walls under boundary conditions typical for a refrigeration and air-conditioning application in a supermarket. The ejector was installed on the test rig to perform a test series that evaluated the outer walls of the ejector with and without insulation. The experimental results were used to validate the proposed CFD model, and a numerical investigation was performed to analyse the influence of heat transfer on ejector performance. The motive nozzle and suction nozzle mass flow rates accuracies were within ±7% and ±15%, respectively. In addition, the proposed CFD model predicted the wall temperatures with ±5 K accuracy for most of the validated points. The heat transfer coefficient of the R744 two-phase flow inside the ejector is presented. The non-adiabatic inner walls degraded ejector performance. The maximum reduction of the mass entrainment ratio reached approximately 13%.

Keywords: carbon dioxide, heat transfer, CFD model, two-phase ejector, heat transfer coefficient, experimental investigation

Nomenclature

c specific heat, J/(kg·K)

E total enthalpy, J/kg

GCI grid convergence index, -

h total specific enthalpy, J/kg

HTC heat transfer coefficient, W/(m²·K)

k thermal conductivity, W/(m·K)

$\dot{m}$ mass flow rate, kg/s

p pressure, Pa

T temperature, K

$\mathbf{u}$ velocity vector, m/s

q heat flux, W/m²

$\dot{W}$ expansion work rate, W

x vapour quality, -

Greek Symbols

α void fraction

χ mass entrainment ratio

Δ absolute difference

δ relative difference, %

η ejector efficiency, %

μ dynamic viscosity, Pa·s

ϕ non dimensional pressure difference, -

ρ density, kg/m³

---

*Michal.Haida@polsl.pl

1. Introduction

Recently legislated regulations of the European Union and the declarations agreed on at the COP21 conference in Paris require replacing a common synthetic refrigerant, i.e., hydro-fluorocarbons (HFCs), with environmentally friendly and natural modern synthetic refrigerants [1].Because of its non-flammability, non-toxicity and satisfactory thermal properties, carbon dioxide (denoted as R744) is one of the most frequently adopted refrigerants in modern commercial refrigeration systems [2]. TModern CO2-based refrigeration systems have been widely introduced in Scandinavia [3] and in northern and central USA [4]. The modification of the R744 refrigeration system configuration facilitates using such systems in hot climates at a competitive energy performance level compared to HFC-based systems [5]. One approach to improving the system coefficient of performance (COP) is the introduction of a two-phase ejector as the primary expansion device [6].

The main aim of the ejector is to entrain the low-pressure suction stream by the supersonic expanded high-pressure motive stream and thus to transfer the kinetic energy of the mixed flow into the pressure energy. Therefore, the outlet pressure of the mixed stream is higher than the suction pressure. The integration of a two-phase ejector into the R744 refrigeration system improves system energy performance up to 18% compared to the reference standard R744 direct expansion system [7]. The CO_2 ejector-based system has been investigated for different applications: heat pump [8], air-conditioning [9] and refrigeration, particularly for supermarkets [10]. These theoretical and experimental investigations indicate a high potential for improving the energy performance of a R744 refrigeration system equipped with a two-phase ejector. However, because of the complexity of the physical phenomena that occur inside the two-phase ejector, the ejector design must be based on a complex mathematical model to work at high efficiency [11].

The CFD model of the R744 ejector based on a homogeneous equilibrium model (HEM) was presented by Lucas et al. [12] and Smolka et al. [13]. Both proposed CFD models assumed adiabatic inner walls. In Lucas et al. [12], the numerical model was implemented using OpenFOAM open-source software, and the investigation was performed with and without the suction flow. The proposed model predicted the motive nozzle mass flow rate and the pressure recovery within an error margin of 10% without the suction flow, and the discrepancy of the pressure recovery increased up to 20% when the suction flow was considered. Moreover, the aforementioned two-phase flow approach was successfully implemented for a numerical investigation of the steam ejector by Giacomelli et al. [14]. The authors compared Wet Steam model available in the commercial software Ansys Fluent together with HEM model. According to the results in [14] the HEM approach overestimates the variations of the main quantities during shocks and expansion process, but is more stable and easy to adapt to various fluids.

Smolka et al. [13] developed a CFD enthalpy-based energy formulation model of the two-phase ejector with adiabatic walls. The authors implemented an enthalpy-based form and real fluid properties from the REFPROP libraries [15] to simulate the supersonic two-phase flow of carbon dioxide. The application range of HEM for the transcritical CO_2 two-phase ejector at typical supermarket conditions was presented by Palacz et al. [16]. The authors stated that motive nozzle and suction nozzle mass flow rate (MFR) accuracies within ±10% were obtained for motive nozzle conditions near and above the critical point. The validated HEM CFD model was used to optimise a two-phase ejector [17]. HEM's high accuracy with respect to transcritical conditions enabled

a numerical investigation of the R744 multi-ejector block by Bodys et al. [18]. A multi-ejector module equipped with four fixed-geometry ejectors was designed and manufactured in cooperation with SINTEF-SUT-DANFOSS based on the CFD model developed by Smolka et al. [13]. In addition, a multi-ejector model was manufactured, and performance mapping of each ejector was performed under refrigeration system operating conditions by Banasiak et al. [19].

Numerical investigations performed using the HEM CFD model of the two-phase ejector facilitate simulating real two-phase flow behaviour under transcritical conditions with high accuracy. However, the analysis of the R744 two-phase ejector in the subcritical region requires a more advanced numerical model. Palacz et al. [20] compared the homogeneous relaxation model (HRM) with HEM to determine the accuracy improvement for operating conditions below the critical point. The authors implemented an additional vapour mass balance equation based on the numerical approach presented by Bilicki and Kestin et al. [21].In addition, the relaxation time was defined according to the definition proposed by Angielczyk et al. [22] for the CO_2 transcritical flow. The authors stated that the motive nozzle and the suction nozzle mass flow rate accuracies of HRM were higher than those of HEM for the subcritical region, and the discrepancy of HRM increased in the transcritical region. Haida et al. [23] presented a modified HRM of the two-phase flow inside the ejector. The authors modified the constant relaxation time coefficients to improve model accuracy. The results for the R744 modified HRM two-phase flow inside the ejector confirmed that the application range of the modified HRM under operating conditions typical for supermarket application was extended compared to the HEM for a motive nozzle pressure up to 60 bar.

Yazdani et al. [24] used a nonhomogeneous mixture model to describe the R744 supercritical fluid flow inside the ejector. The aforementioned model implemented additional set of equations describing the phase change caused by boiling and cavitation. The $k - \omega$ SST turbulence model was applied. The numerical results in the form of pressure profiles agreed well with the measured data. Furthermore, the difference between the simulated and measured mass entrainment ratios (MER) was below 10%. Liao et al. [25] investigate the two-phase flow in water-steam converging diverging nozzle by use of the two-fluid model incorporating drag and non-drag forces. In addition, the pressure jump across the interface was omitted and only inter-phase heat transfer induced the phase change. the authors stated that the satisfactory prediction of the mass flow rate and cross-section averaged parameters was obtained when compared to the experimental data. Le et al. [26] proposed a two-phase mixture CFD model to simulate flashing flow of the vaporised water in a converging-diverging nozzle. The thermal non-equilibrium effect was implemented by use of the boiling delay model. The numerical results were compared to the experimental data given from literature followed by the detailed sensitivity analysis. The authors stated that the aforementioned model obtained acceptable accuracy of the global and local flow dynamics quantities.

The accuracy of the CFD two-phase ejector model is related to the defined turbulence approach. Croquer et al. [27] performed investigation of the $k-\epsilon$-based and $k-\omega$-based turbulence models for a R134a ejector. The authors stated that the $k - \epsilon$ with high-Reynolds number formulation and $k - \omega$ SST model in its high- or low-Reynolds number formulation obtained χ deviation of 4%. The similar comparison of turbulence models was also done by Mazzelli et al. [28] for 2D and 3D CFD air ejector model with rectangular cross-section. The investigation was done for $k-\epsilon$, $k-\epsilon$ Realizable, $k-\omega$ SST and Reynolds Stress Model. Besagni et al. [29] compared aforementioned turbulence models with additional $k-\epsilon$ RNG and Spalart-Allmaras turbulence approaches for an air ejector. The detailed investigation for the foregoing turbulence models with different near-wall modelling options for a steam ejector was presented by Besagni et al. [30]. Based on the results presented in [28, 29, 30] the $k - \omega$ SST showed the best agreement in terms of local and global supersonic compressible flow inside the aforementioned ejectors. Varga et al. [31] compared $k-\epsilon$-based, $k-\omega$-based and Transition SST turbulence models applied to the steam CFD model. The authors stated that Transition SST model obtained best accuracy of COP and the critical back pressure with the average discrepancy of 4% and 1.4%, respectively.

In addition to the numerical investigation of the homogeneous fluid flow assumptions and turbulence models, the influence of friction loss on supersonic ejector performance has been analysed. Brezgin et al. [32] investigated the roughness effect on a supersonic ejector using a CFD model for organic working fluid R245fa. The authors stated that for given boundary conditions and ejector geometry, the performance rapidly decreased when a critical roughness height was exceeded. Mazzelli et al. [33] presented numerical simulations of the R245fa ejector for an industrial chiller application based on an internal dynamics analysis. The authors concluded that surface roughness strongly influenced the mass flow rate prediction of the CFD model compared to experimental data, particularly for off-designed operating conditions. A similar conclusion was reported by Zhang et al. [34], who nu-

merically investigated the effect of friction on R134a supersonic ejector performance and found that an increase in surface roughness rapidly decreased the mass entrainment ratio. In addition, the higher roughness of the ejector wall surfaces changed the temperature and the Mach number of the flow inside the ejector.

Milazzo et al. [35] presented the influence of a different constant wall temperature and roughness on R245fa ejector performance. The authors performed numerical simulations near the critical point of the two-dimensional axisymmetric CFD ejector model. The change in the constant wall temperature resulted in a different mass entrainment ratio. Additionally, the heat transfer coefficient (HTC) along the axis at the ejector wall was presented in [35]. The authors stated that the heat loss towards the ambient should be considered for a precise sizing of the condenser and that the ejector's inner surfaces cannot be considered adiabatic.

In addition to friction loss and inner wall temperature investigations of the ejector, non-adiabatic wall analysis has been performed for different expansion devices, e.g., a capillary tube. Numerical simulations of the R134a flow through non-adiabatic capillary tubes were performed in [36]. The authors proposed a theoretical mathematical model to consider the heat exchange between walls and a single or a two-phase flow of the working fluid. The model was validated and used to design a non-adiabatic capillary tube. Agrawal et al. [37] investigated the effect of a gas cooler and evaporator temperatures on R744 non-adiabatic capillary tube performance. The analysis also considered capillary tube diameter and heat exchanger length. The authors stated that a shorter inlet adiabatic capillary length and a longer non-adiabatic capillary length increased the heat transfer rate.

The main aim of this paper is to investigate the influence of heat transfer within a CO_2 two-phase ejector on ejector performance. To the best knowledge of the authors, there is no such analysis in the literature. Therefore, numerical simulations were performed of forced convection, heat conduction in the ejector body and the free convection of the sourroundings. The CO_2 two-phase flows within the ejector were simulated based on the modified HRM proposed by Haida et al. [23]. The R744 two-phase ejector was designed and manufactured in Gliwice, Poland to experimentally investigate the inner wall temperatures. To validate the developed CFD model, an experimental test series was performed on the CO_2 ejector test rig at the NTNU/SINTEF Energy Research laboratory in Trondheim, Norway. The sensitivity analysis of the wall conductivity, roughness, HTC of the free stream air and turbulence model on the inner wall temperature distribution was done. In addition, the heat transfer coefficient of the motive nozzle, suction nozzle and mixed streams under different operating conditions is presented.

2. R744 two-phase ejector for inner walls temperature measurement

Figure 1 presents the R744 two-phase ejector designed and manufactured by Institute of Thermal Technology in Gliwice, Poland, to facilitate measuring the wall temperature close to the inner surface of the ejector. The ejector was assembled from three parts: the motive nozzle, the suction nozzle together with the mixer and the diffuser and finally the outlet port. The suction nozzle was designed as a tangential inlet to connect the nozzle with the test rig. Therefore, the suction stream swirled in the suction chamber. Moreover, the aforementioned part was defined to maintain a cross-section area in the converging part of the suction nozzle. Stainless steel was used to manufacture the motive nozzle and brass for the remaining parts. Eight screws were used to bolt the ejector. Swagelok connectors were used to connect the inlet and outlet ports with the test rig pipelines. In addition, thirteen small holes were drilled throughout the ejector to facilitate inserting thermocouples for inner wall temperature measurements.

The placement of the temperature probes is shown in Figure 2. The position of the sensors was selection to avoid the influence of the nearest thermocouple on a single measurement. Therefore, two characteristic sections were selected (Figure 2(a)). The thermocouples were placed to measure the wall temperature in the motive inlet, in the suction inlet, between the converging-diverging nozzle and the converging suction nozzle, in the pre-mixer, in the mixer and in the diffuser. The distance between the inner wall surface and the probes was 2 mm. The total number of thermocouple channels was thirteen. The main geometric parameters of the two-phase ejector are presented in Table 1. The ejector was designed based on the dimensions presented by Banasiak et al. [38] for the smallest ejector called *Case 1*.

The designed and manufactured R744 ejector allows for the experimental investigation of the inner wall temperature profile at different operating and ambient conditions. Hence, the ejector was firstly tested by performing the pressure test using a nitrogen at 140 bar to avoid any leakage inside the ejector before it was connected to the
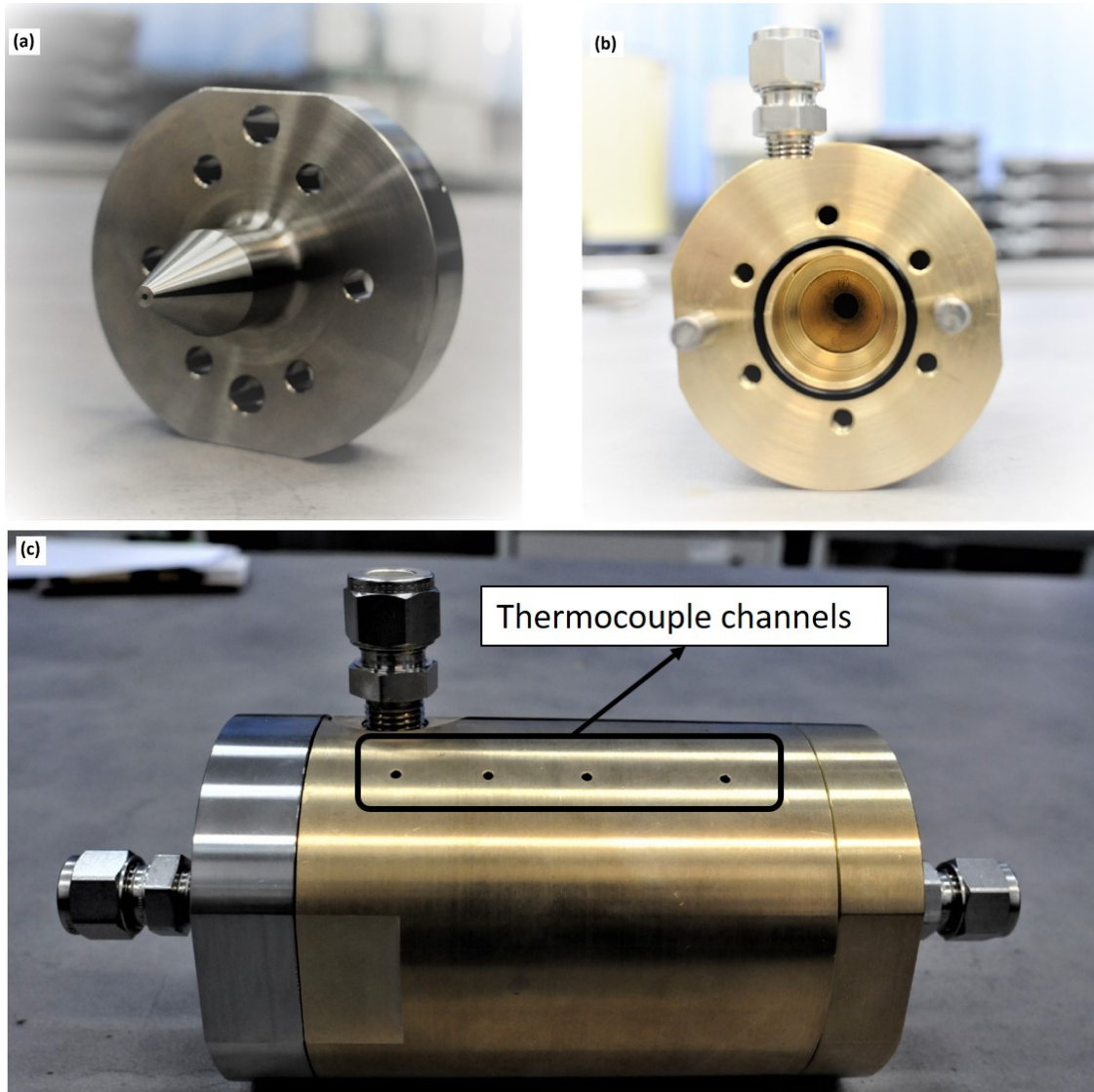
4

Figure 1: The R744 two-phase ejector for inner walls temperature measurement: (a) the motive nozzle; (b) the suction nozzle together with the mixing chamber and the diffuser; (c) the assembly with the thermocouples channels.

system. Then, the ejector was implemented to the test rig at the SINTEF/NTNU laboratory in Trondheim, Norway for a test campaign.

3. R744 two-phase ejector test series

The test rig was a R744 vapour compression unit, which facilitates the implementation of different expansion devices, e.g., an ejector, an expansion valve or a capillary tube [8, 13, 39, 40]. The simplified lay-out of the test rig with the measurement equipment was shown in Figure 3. The R744 loop of the system contains a semi-hermetic reciprocating compressor, two brazed plate heat exchangers working as a gas cooler (gc) and an evaporator (ev), an internal heat exchanger (IHX), a separator and the ejector for inner walls temperature measurement. The compressor was connected to the inverter, whereby the discharge pressure was set to accommodate different compressor frequencies. The discharge pressure varied in the range from 70 bar to 110 bar to analyse the ejector
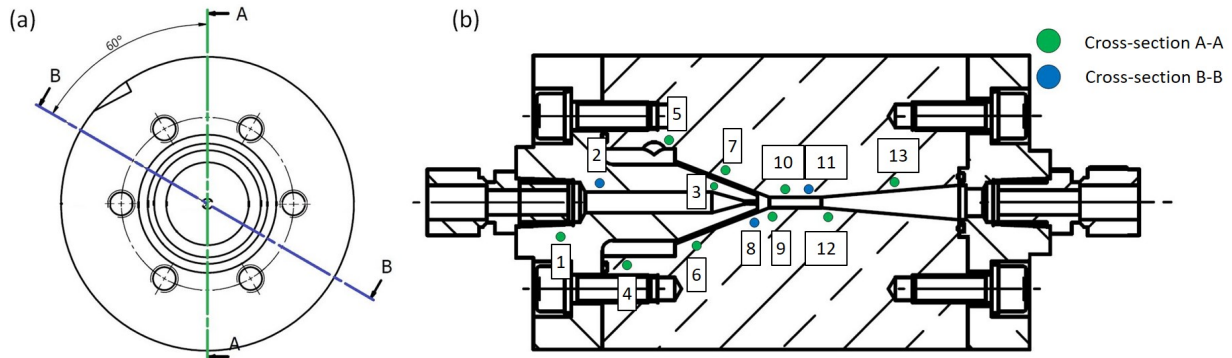
5

Figure 2: The thermocouples localisation in the R744 two-phase ejector: (a) selected cross-sections for thermocouple channels; (b) probes localisation along ejector axis.

Table 1: The main geometry parameters of the R744 two-phase ejector.

Parameter name	Unit	Dimension
Motive nozzle inlet diameter	10^{-3} m	6.00
Motive nozzle throat diameter	10^{-3} m	0.75
Motive nozzle outlet diameter	10^{-3} m	1.05
Motive nozzle converging angle	°	30.00
Motive nozzle diverging angle	°	2.00
Suction chamber diameter	10^{-3} m	31.00
Suction chamber length	10^{-3} m	21.10
Suction converging angle	°	42.00
Pre-mixer length	10^{-3} m	3.50
Mixer length	10^{-3} m	15.00
Diffuser outlet diameter	10^{-3} m	8.00
Diffuser angle	°	5.00
Outer wall diameter	10^{-3} m	75.00
Outer wall length	10^{-3} m	155.00
Outer brass wall length	10^{-3} m	130.00

performance for transcritical and close to critical point operating conditions. The evaporator pressure was controlled by the metering expansion valve. The evaporation temperature was set to -10°C and 0°C typical for cooling application and air-conditioning application in the supermarket [41]. The two-phase ejector was connected to the test rig using Swagelok connectors. Therefore, the expanded motive stream and entrained suction stream entered the separator tank at a higher pressure than the evaporation pressure.

The auxiliary glycol loops (gl) were used to provide cooling and heating in the gas cooler and in the evaporator. Each glycol loop is equipped with the glycol pump, an electric heat exchanger (EHX) and a glycol tank. The concentration of the glycol was set to approximately 50% to ensure the required operating conditions of the ejector. In addition, the test rig was equipped with the oil recovery loop to ensure the limitation of the oil concentration in the working fluid and ensure the safety oil level in the compressor.

The test facility was fully equipped with pressure, temperature and the mass flow-rate sensors, for which the

accuracies were adopted from the product data sheets. The temperature was measured in the nozzles and outlet collectors by PT100 class A resistance thermometers with an accuracy of $\pm(0.15 + 0.002\ T)$, where T is the temperature in $^{\circ}$C. The wall measurements were performed using T-type calibrated thermocouples with a reading accuracy of $\pm0.75\%$. A piezoelectric transmitter was used to measure the pressure, with a reading accuracy of $\pm0.3\%$. MFR measurement was performed using Coriolis RHM04 and RHM06 transducers, and the reading accuracy was $\pm0.2\%$. The output signals from the sensors installed in the test rig were processed and transmitted using a National Instruments control unit to the LabView system. The data were exported as a CSV standard to the uncertainty analysis.
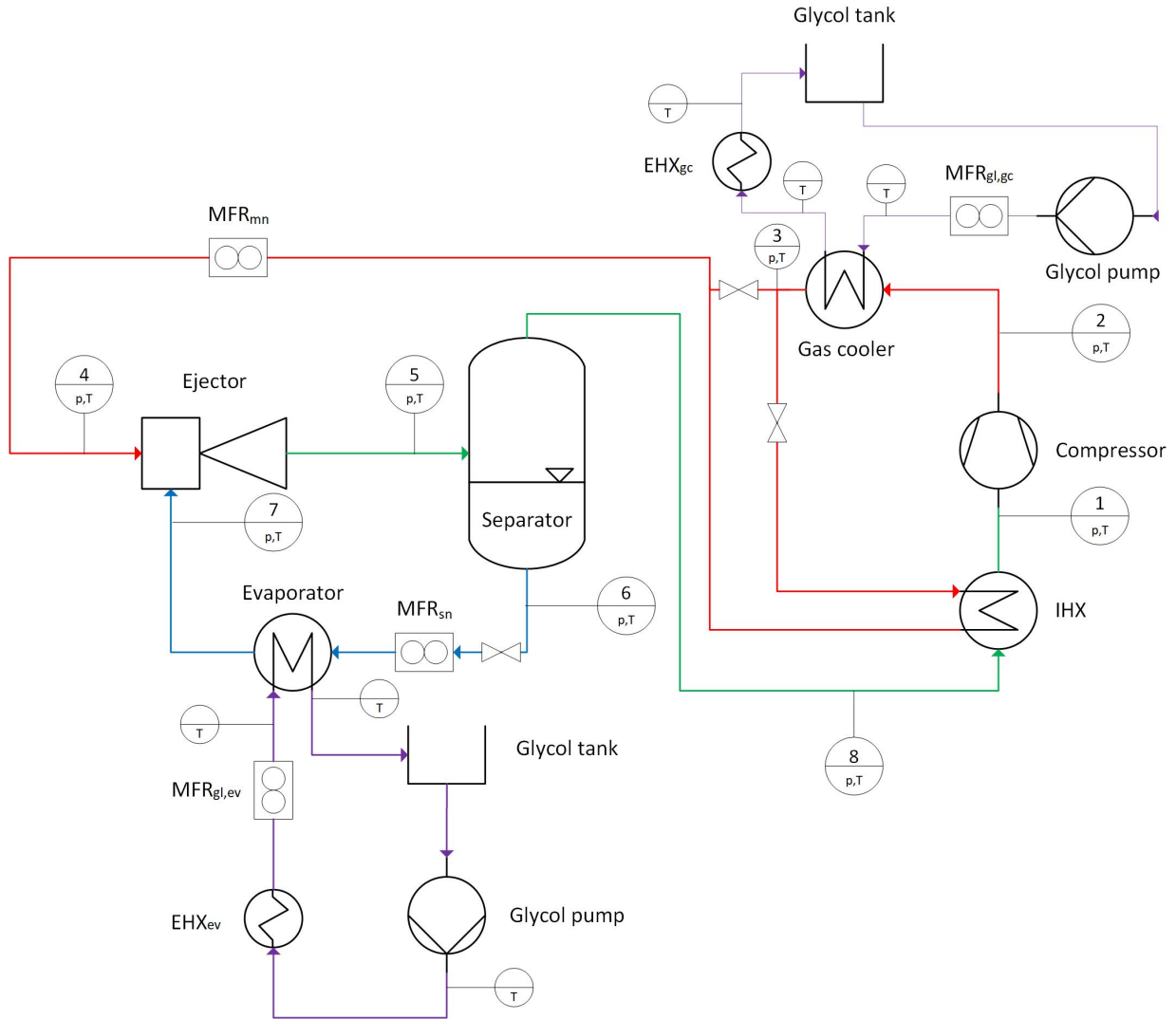

Figure 3: The simplified P&ID diagram of the R744 vapour compression test rig equipped with the ejector for inner walls temperature measurement: EHX - electric heat exchanger, IHX - internal heat exchanger.

The test series was performed to determine the transcritical and near-critical point operating conditions of the motive nozzle for a set of temperature differences between the motive nozzle and the suction nozzle. The experimental results were used for a mesh sensitivity analysis and to validate the R744 two-phase ejector CFD model.

$$\Delta T = T_{MN} - T_{SN} \tag{1}$$

216 where Δ is the absolute difference and T is the temperature in $^{\circ}$C of the motive nozzle (MN) and the suction nozzle
217 (SN). Moreover, the test campaign of the R744 two-phase ejector was done for two variants:

218 • Fully insulated outer walls

219 • The outer walls without an insulation

220 The foregoing variants allows the influence of the non-adiabatic outer walls on the R744 two-phase flow and
221 the ejector performance. The experimental results were used for a mesh sensitivity analysis and a validation pro-
222 cedure of the R744 two-phase ejector CFD model.

223 **4. Numerical approach**

224 The proposed numerical model of the CO_2 two-phase ejector simulated two-phase supersonic flow behaviour
225 together with the heat transfer process that occurs between the high-temperature motive fluid and low-temperature
226 suction fluid and inside ejector walls. In addition, the different ambient conditions and the conductivity of the
227 outer ejector walls were considered in the proposed model. The CFD model approach together with the computa-
228 tional procedure was described in Section 4.1. The influence of the heat transfer on the ejector performance can
229 be shown by use of HTC. Hence, the calculation of HTC for each ejector component was presented in Section 4.2.

230 *4.1. CFD model*

The homogeneous relaxation flow assumption simplifies the numerical model to the equations that govern
the mass, momentum, energy and vapour mass balance of the relaxation mixture. In addition, steady-state com-
putations were performed for each operating condition. Therefore, all of the time derivatives in the governing
equations were omitted. The mass balance is described as follows:

$$\nabla \cdot \left(\bar{\rho} \tilde{\mathbf{u}} \right) = 0 \tag{2}$$

where the symbols ($\bar{}$) and ($\tilde{}$) denote the Reynolds- and Favre-averaged quantities, respectively. In addition, ρ
is the fluid density in kg/m^3 and $\mathbf{u}$ is the fluid velocity vector in m/s. The momentum balance is defined by the
following equation:

$$\nabla \cdot \left(\bar{\rho} \tilde{\mathbf{u}} \tilde{\mathbf{u}} \right) = -\nabla \bar{p} + \nabla \cdot \tilde{\tau} \tag{3}$$

where p is the pressure of the mixture fluid in Pa and τ is the stress tensor in N/m^2. The vapour mass balance
equation is described in the following form [21]:

$$\nabla \cdot \left(\tilde{\rho} \tilde{x} \right) = -\tilde{\rho} \left(\frac{\tilde{x} - \tilde{x}_{eq}}{\tilde{\theta}} \right) \tag{4}$$

where x is the instantaneous vapour quality of the two-phase flow, x_{eq} is the vapour quality at the equilibrium
state and θ is the relaxation time in s. According to Haida et al. [23] the relaxation time for CO_2 two-phase flow is
defined by the following equation:

$$\tilde{\theta} = \theta_0 \cdot \tilde{\alpha}^a \cdot \bar{\phi}^b \begin{cases} \theta_0 = 1.0e-07 & a = 0.0 & b = 0.0 & p_{mn} = 73.77 \text{ bar} \\ \theta_0 = 9.0e-06 & a = -0.67 & b = -1.73 & 59 \text{ bar} \leq p_{mn} \leq 73.77 \text{ bar} \\ \theta_0 = 1.5e-06 & a = -0.67 & b = -2.00 & p_{mn} \leq 59 \text{ bar} \end{cases} \tag{5}$$

where θ_0, a and b are the constant relaxation time coefficient defined for different motive nozzle pressure ranges
p_{mn}, α is the void fraction and ϕ is the non-dimensional pressure difference defined as follows:

$$\tilde{\alpha} = \frac{\tilde{x} \cdot \bar{\rho}}{\bar{\rho}_v} \tag{6}$$

$$\bar{\phi} = \left| \frac{\bar{p}_{sat} - \bar{p}}{p_{crit} - \bar{p}_{sat}} \right| \tag{7}$$

8

where ρ_v is the density of the saturated vapour, p_{sat} is the saturation pressure based on the motive nozzle inlet conditions and p_{crit} is the critical pressure of CO_2. According to Smolka et al. [13], the temperature-based form of the energy equation can be replaced by the enthalpy-based form. Hence, the energy balance of the R744 two-phase flow can be defined as follows:

$$\nabla \cdot \left(\bar{\rho} \tilde{\mathbf{u}} \tilde{E} \right) = \nabla \cdot \left[\left(\frac{k_f}{\frac{\partial h}{\partial T}} \right)_p \nabla \tilde{h} - \left(\frac{k_f}{\frac{\partial h}{\partial T}} \right)_p \left(\frac{\partial h}{\partial p} \right)_T \nabla \bar{p} + \bar{\tau} \cdot \tilde{\mathbf{u}} \right] + \bar{q}_v \tag{8}$$

where T is the mixture temperature in K, k_f is the fluid thermal conductivity in W/(m·K), q_v is the heat source in W/m^3 and E is the total specific enthalpy in J/kg defined as a sum of the specific mixture enthalpy and the kinetic energy:

$$\tilde{E} = \tilde{h} + \frac{\tilde{u}^2}{2} \tag{9}$$

where h is the mixture specific enthalpy in J/kg. The enthalpy-based form of the energy equation let to define fluid properties as a function of the pressure and specific enthalpy:

$$\{\rho, \mu, k_f, c_p\} = f(p, h) \tag{10}$$

where μ is the dynamic viscosity in Pa·s and c_p is the specific heat in J/(kg·K). The pressure-based boundary conditions were used for the motive nozzle and suction nozzle inlets and the outlet of the two-phase ejector. The heat transfer in the ejector walls was simulated using heat conduction equation in the following form:

$$\nabla (k_w \cdot \nabla T) = 0 \tag{11}$$

where k_w is the ejector wall thermal conductivity in W/(m·K). The foregoing heat conduction equation was implemented using the user-defined scalar (UDS) in Ansys Fluent software. The conjugate heat transfer method was used to couple heat transfer with the two-phase flow based on fourth kind boundary conditions. The near-wall fluid temperature was defined as a boundary condition of the ejector inner walls for the conductivity process. In two-phase flow, the local heat rate obtained due to the conductivity process between the ejector walls was implemented in the enthalpy-based equation as a heat source at each fluid cell. Therefore, the model defined the continuity of temperature and heat flux at the interface between the fluid and the solid sub-domains. Additionally, the fourth kind boundary condition facilitated defining the inner ejector walls as non-adiabatic or adiabatic walls. The outer ejector walls were defined as insulated walls with heat flux equal to zero or using the convection-type boundary condition. The ambient temperature was measured during the test series, and the heat transfer coefficient of air was assumed to be 5 W/(m^2·K). As a result of the different heat transfer boundary conditions on the inner and outer ejector walls, four heat transfer variants was defined as follows:

- HT-1 - adiabatic inner walls and adiabatic outer walls

- HT-2 - non-adiabatic inner walls and adiabatic outer walls

- HT-3 - adiabatic inner walls in the motive nozzle part, non-adiabatic inner walls in the suction nozzle, mixer and diffuser and non-adiabatic outer walls

- HT-4 - non-adiabatic inner and outer walls

Finally, the coupled mathematical model of the two-phase flow together with the non-adiabatic ejector walls was defined. An implementation of the heat transfer in the ejector walls increased the computational time of the CFD model. As an example, the total computational time for 3-D CFD model was of approximately 14 hours with and approximately 10 hours without the ejector walls heat transfer, respectively. The difference between the solving times was affected by the solid domain consideration in the proposed model. A numerical approach was implemented in the discretised domain of the R744 two-phase ejector to perform the numerical computations under specified operating conditions, heat-transfer wall conditions and ambient conditions. The set of the boundary

Table 2: The set of the boundary conditions types in the R744 two-phase ejector.

Boundary name	Flow boundary	Turbulence boundary	Solid boundary
MN Inlet	$P_{MN}, T_{MN}, h_{MN}, q_{MN}$	Hydraulic diameter, turbulence intensity	-
SN Inlet	$P_{SN}, T_{SN}, h_{SN}, q_{SN}$		
Outlet	P_{out}	-	
Steel inner wall	Conjugate heat transfer	Wall function	Conjugate heat transfer
Brass inner wall			
Steel outer wall	-	-	Heat flux
Brass outer wall			

conditions types was shown in Table 2. The boundary conditions were defined for flow, turbulence and solid walls boundaries types.

The partial differential equations of the mathematical model were solved based on the PRESTO scheme for the pressure discretisation and the second-order upwind scheme for the other variables considered in the CFD model. The coupled method was employed for the coupling of the pressure and velocity fields. The set of the numerical schemes was listed in Table 3

Table 3: The set of the numerical schemes of the CFD model.

Discretisation	Scheme
Pressure-velocity coupling	Coupled algorithm [42]
Gradient	Green-gauss cell based
Momentum	Second-order upwind
Pressure	PRESTO! [42]
Density	Second-order upwind
Energy [13]	
Vapour mass balance [23]	
Heat conduction	
Turbulence kinetic energy	Second-order upwind
Specific dissipation rate	
Intermittency (Transition SST)	
Momentum thickness Reynolds number (Transition SST)	
Reynold stresses (Reynold Stress Model)	

The turbulence model was chosen based on the CFD model verification presented and discussed in Section 5.2. The wall roughness was set to 2 µm according to the ejector manufacturers. The real fluid properties of R744 were approximated based on the data obtained using the REFPROP libraries [15]. Moreover, the physical properties of the CO_2 two-phase flow were calculated as a function of the pressure and specific enthalpy due to the enthalpy-based energy formulation defined in Eq. (8):

$$\{\rho, c_p, k_f, \mu\} = f(p, h) \tag{12}$$

10

where c_p is the specific heat capacity in J/(kg·K) and μ is the dynamic viscosity in Pa·s. The foregoing function allows for the R744 flow calculation in single- and two-phase flow conditions for subcritical, transcritical, and close to the critical operating conditions [13, 16]. The thermal conductivity of the stainless steel and brass was set to 16 W/(m·K) and 109 W/(m·K), respectively.

The proposed CFD model was used to analyse heat transfer in the R744 two-phase ejector and the influence of the ejector design and the temperature difference between both nozzles on ejector performance. The ejector work is described using the mass entrainment ratio and ejector efficiency definitions. The mass entrainment ratio is the ratio between the suction nozzle MFR and the motive nozzle MFR:

$$\chi = \frac{\dot{m}_{SN}}{\dot{m}_{MN}} \tag{13}$$

where χ is the mass entrainment ratio and $\dot{m}$ is the mass flow rate of the motive nozzle (MN) and the suction nozzle (SN). The ejector efficiency was defined by Elbel et al. [6] as a ratio of the amount of the recovered ejector expansion work rate to the maximum possible expansion work rate recovery potential:

$$\eta_{ej} = \frac{\dot{W}_{rec}}{\dot{W}_{rec,max}} = \chi \cdot \frac{h(p_{out}, s_{SN}) - h(p_{SN}, s_{SN})}{h(p_{out}, s_{MN}) - h(p_{MN}, s_{MN})} \tag{14}$$

where η_{ej} is the ejector efficiency, $\dot{W}$ is the expansion work rate in W and s is the specific entropy in J/(kg·K). In this paper, the mass entrainment ratio and ejector efficiency were used to analyse the heat-transfer influence on the R744 two-phase flow performance under operating conditions typical for refrigeration and air-conditioning applications. Therefore, the CFD two-phase ejector model was validated with the experimental data to ensure the high accuracy of the numerical model. The accuracy of the proposed CFD model was calculated as the relative error between the experimental data and the model result:

$$\delta_{var} = \frac{var_{CFD}}{var_{EXP}} - 1 \tag{15}$$

where δ_{var} is the relative error of the selected two-phase flow parameter obtained by the CFD model or given by the experimental data.

4.2. Heat transfer coefficient calculations

The heat transfer behaviour between the CO_2 two-phase flow and the ejector walls can be determined by HTC. The evaluation of the heat transfer coefficient within the R744 ejector facilitated the proper selection of the wall material and the consideration of the heat transfer in ejector shape design. In the motive nozzle, HTC can be defined in the following form:

$$HTC = \left(\frac{\dot{q}}{|T_{wall} - T_{stream}|} \right) \tag{16}$$

where HTC is the heat transfer coefficient in W/(m²·K) and $\dot{q}$ is the heat flux in W/m². The temperature T_{wall} is the local wall temperature and T_{stream} is the local fluid temperature. The heat flux was given for each inner wall, whereas the local wall temperature and the local fluid temperature were taken from the inner walls and close to the inner walls, respectively. The Newton's law of cooling presented in Eq. (16) was also used for the suction nozzle, the mixer and the diffuser part of the two-phase ejector.

Finally, the proposed CFD model was verified and validated based on the experimental data obtained for the manufactured R744 two-phase ejector. Therefore, the experimental results and the numerical investigation are presented in this paper to analyse the heat transfer in the CO_2 two-phase ejector.

5. Results and discussion

5.1. Experimental results

Table 4 presents the experimental data of the R744 two-phase ejector with insulated outer walls. The motive nozzle boundary conditions varied in a range from approximately 75 bar and 290 K to over 106 bar and 306 K.

₃₀₂ Therefore, the investigated region included ejector operation under transcritical and near-critical operating con-
₃₀₃ ditions. The suction nozzle pressure was between approximately 27 bar and 37 bar, and the temperature was
₃₀₄ above the evaporation temperature for each boundary condition. Additionally, the pressure difference between
₃₀₅ the ejector outlet and the suction nozzle was below 4 bar. The test series was performed with ΔT in a range from
₃₀₆ 8 K to approximately 28 K to investigate the influence of the nozzle temperatures on the wall temperature dis-
₃₀₇ tribution. Finally, the two-phase ejector exhibited a mass entrainment ratio between approximately 0.4 and 0.56
₃₀₈ as the result of the small difference between the ejector outlet and the suction nozzle. In addition, the highest
₃₀₉ ejector efficiency was approximately 12% for #AD8 at a motive nozzle pressure above 90 bar and the highest ΔT of
₃₁₀ approximately 28 K. Due to the fact that the presented investigation was strongly focused on the different ΔT and
₃₁₁ motive nozzle conditions, the ejector efficiency was a secondary effect of the experimental tests.

Table 4: The set of the experimental data of the R744 two-phase ejector with adiabatic (AD) outer walls.

BC	P_{MN}	T_{MN}	P_{SN}	T_{SN}	P_{out}	ΔT	χ	η_{ej}
	bar	K	bar	K	bar	K	-	%
#AD1	87.4	294.8	38.8	283.2	39.5	11.6	0.6	6.1
#AD2	90.4	294.2	37.0	280.4	39.5	13.8	0.6	9.6
#AD3	83.7	302.3	33.4	283.9	34.9	18.4	0.5	9.2
#AD4	106.3	306.9	36.6	280.5	39.0	26.4	0.6	11.8
#AD5	91.4	300.0	35.8	291.8	37.5	8.2	0.5	11.2
#AD6	78.9	296.8	33.6	284.4	35.0	12.3	0.4	9.7
#AD7	75.3	299.3	27.5	283.9	29.0	15.4	0.4	9.9
#AD8	97.1	304.9	27.3	276.9	29.7	27.9	0.5	12.1

₃₁₂ Table 5 presents the experimental data of the R744 two-phase ejector without outer wall insulation. Similar
₃₁₃ to the results presented in Table 4, the motive nozzle was in a range of approximately 71 bar to over 100 bar.
₃₁₄ However, the suction nozzle pressure varied between 24 bar and 28 bar with the pressure difference between the
₃₁₅ ejector outlet below 4 bar. To determine the influence of the two-phase ejector environment on its performance,
₃₁₆ the ambient temperature was measured. In the investigation presented in Table 5, the ambient temperature varied
₃₁₇ slightly between 297 K and 298 K, and ΔT ranged from 15 K to approximately 33 K. The mass entrainment ratio
₃₁₈ of the R744 ejector with non-adiabatic outer walls was between approximately 0.37 and 0.46. Similar to the test
₃₁₉ series performed with insulated outer walls, the best performance of the R744 two-phase ejector was reached
₃₂₀ under boundary condition #NAD8 with the motive nozzle pressure above 100 bar and with the highest ΔT of
₃₂₁ approximately 32 K.

₃₂₂ The operating conditions given from the test campaign were presented in Figure 4. The motive nozzle condi-
₃₂₃ tions shown in Figure 4(a) were located close to the critical point, e.g. #NAD1 and #NAD2, but most of the in the
₃₂₄ transcritical conditions below 110 bar. In addition, the test points were obtained for the motive nozzle tempera-
₃₂₅ ture in the range from 293.15 K to 313.15 K. The results given from the adiabatic test series were reached for the
₃₂₆ suction nozzle in the range from 26 bar to 40 bar, as shown in Figure 4(b). The suction nozzle conditions of the
₃₂₇ non-adiabatic test points varied in the range from 25 bar to 30 bar. Moreover, the suction nozzle temperature of
₃₂₈ both test series was above 273.15 K and below 293.15 K.

₃₂₉ Figure 5 presents the experimental results for the wall temperature distribution of the R744 two-phase ejector.
₃₃₀ The placement of each thermocouple was numbered (Figure 2). The wall temperature distribution is presented
₃₃₁ under two boundary conditions for the ejector with adiabatic outer walls (#AD1 and #AD5) and under two bound-
₃₃₂ ary conditions with non-adiabatic outer walls (#NAD2 and #NAD7) defined in Table 4 and in Table 5. The selected
₃₃₃ boundary conditions obtained different ΔT between 8 K and 26 K and different motive nozzle temperatures in a
₃₃₄ range from approximately 295 K to 306 K. It can be observed that the motive nozzle reached a higher temperature
₃₃₅ than the second part of the ejector assembly. In addition, the removal of the adiabatic outer wall influenced the

Table 5: The set of the experimental data of the R744 two-phase ejector with non-adiabatic (NAD) outer walls.

BC	P_{MN}	T_{MN}	P_{SN}	T_{SN}	P_{out}	T_{amb}	ΔT	χ	η_{ej}
	bar	K	bar	K	bar	K	K	-	%
#NAD1	71.8	300.9	24.8	285.6	26.5	297.1	15.4	0.4	8.9
#NAD2	71.4	301.0	24.5	274.7	25.9	296.7	26.3	0.4	9.0
#NAD3	83.0	303.0	27.6	284.5	29.6	297.4	18.6	0.4	11.5
#NAD4	80.5	302.5	26.4	277.5	28.4	297.5	24.9	0.4	11.0
#NAD5	94.8	301.5	26.5	284.6	28.3	297.5	16.9	0.5	10.5
#NAD6	92.5	301.7	25.6	273.6	27.4	297.9	28.1	0.5	9.9
#NAD7	101.0	306.3	25.6	284.6	28.4	297.2	22.2	0.4	12.9
#NAD8	100.6	306.8	25.4	274.4	28.3	298.2	32.4	0.4	13.4
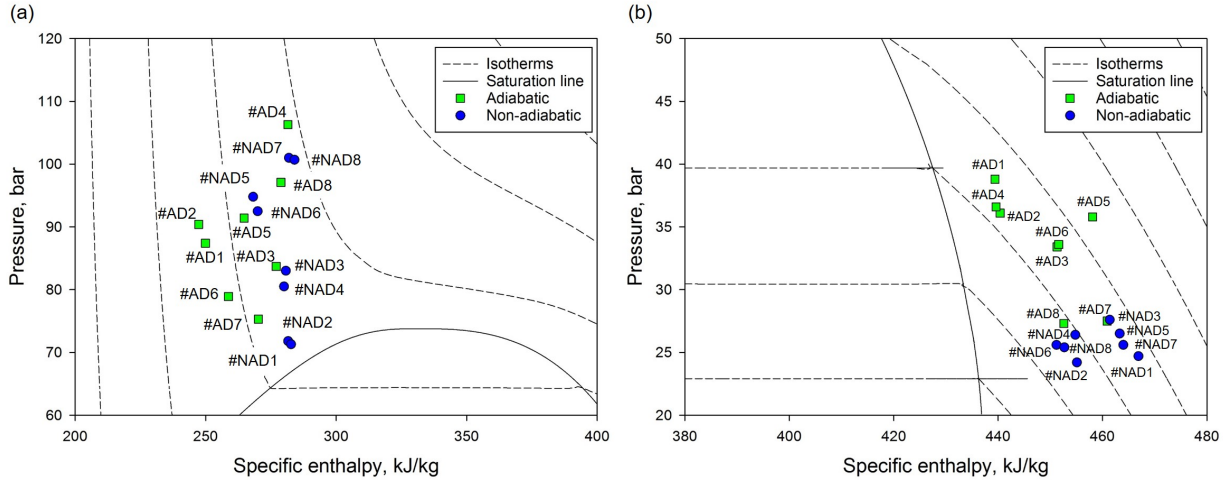
Figure 4: The pressure-specific enthalpy diagram with operating conditions defined in Table 4 and in Table 5: (a) motive nozzle; (b) suction nozzle.

temperature distribution close to the inlet of the motive nozzle. The second thermocouple exhibited a slightly lower temperature than the first probe under boundary conditions #NAD2 and #NAD7. The wall temperature of the suction nozzle and the mixer together with the diffuser decreased along the ejector axis. It can be observed that the thermocouples located at the end of the mixer and in the diffuser reached similar temperatures. Therefore, the influence of heat transfer on the two-phase flow behaviour appeared between the two nozzles and in the pre-mixing section with respect to the wall temperature distribution.

The experimental test series performed on the R744 two-phase ejector confirmed the influence of the ambient conditions on the wall temperature distribution under different operating conditions, particularly on the motive nozzle. Therefore, the investigation of the heat-transfer influence on ejector performance using the proposed CFD enabled us to determine the best solution for ejector efficiency.

5.2. Sensitivity analysis of the CFD model

As a result of the tangential suction inlet shape of the two-phase ejector, the numerical analysis was done based on the three-dimensional CFD model. The 3-D two-phase ejector geometry was discretised with a fully structured grid with a minimum orthogonal quality over 0.6. The numerical grid considered three domains with respect to
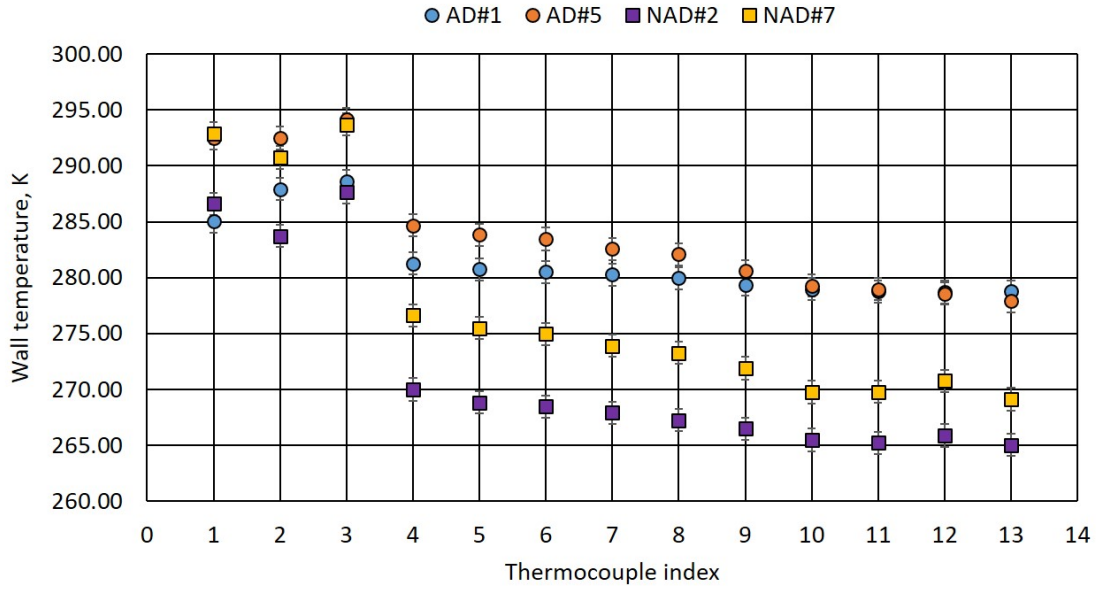
13

Figure 5: The wall temperature measurements of the R744 two-phase ejector at boundary conditions #AD1, #AD5, #NAD2 and #NAD7 defined in Table 4 and in Table 5.

the two-phase flow and two ejector walls with different materials. The numerical mesh was presented in Figure 6 for each domain and in the cross-section defined by a red dotted line in Figure 6(a) and Figure 6(b).

The results of the ejector mesh independence study are presented in Figure 7. The mesh sensitivity analysis was performed to avoid the influence of the ejector mesh on the global and local parameters, i.e., MFRs and temperature. Therefore, the motive nozzle and the suction nozzle MFRs are presented. In addition, the local temperatures of the motive nozzle are shown in Figure 7. Moreover, the local temperatures of the motive nozzle part were defined in Figure 2. All parameters obtained the similar values for the number of elements above approximately 2.5 millions elements. All parameters exhibited similar values for the number of elements above approximately 2.5 million. It can be observed that the suction nozzle MFR and temperature T_2 located close to the converging-diverging nozzle were the most sensitive parameters and strongly related to the number of mesh elements.

The mesh refinement was performed by increasing the element number at the selected geometrical parameters describing the R744 two-phase ejector as shown in Figure 7(b). The mesh refinement was done mostly in the converging-diverging part of the motive nozzle, converging part of the suction chamber, pre-mixer, mixer and the diffuser. The selected geometrical parameters presented in the cross-sectional view of the ejector defined the element number in the whole mesh with consideration of the boundary layer. In addition, the wall y^+ was calculated during the mesh sensitivity analysis to define the simulation of the near wall two-phase flow for each generated numerical grid. The results of the wall y^+ analysis were the following for the tested meshes:

- $y^+ \approx 45.0$ for 1.5 million elements

- $y^+ \approx 11.0$ for 2.0 million elements

- $y^+ \approx 3.2$ for 2.5 million elements

- $y^+ \approx 0.3$ for 3.0 million elements

The wall y^+ below 5.0 for the mesh above 2.0 millions elements confirmed high accuracy of the CFD results in the whole ejector, especially within the boundary layer. Finally, the numerical grid with 2.5 million elements was chosen for the validation procedure and further investigations.
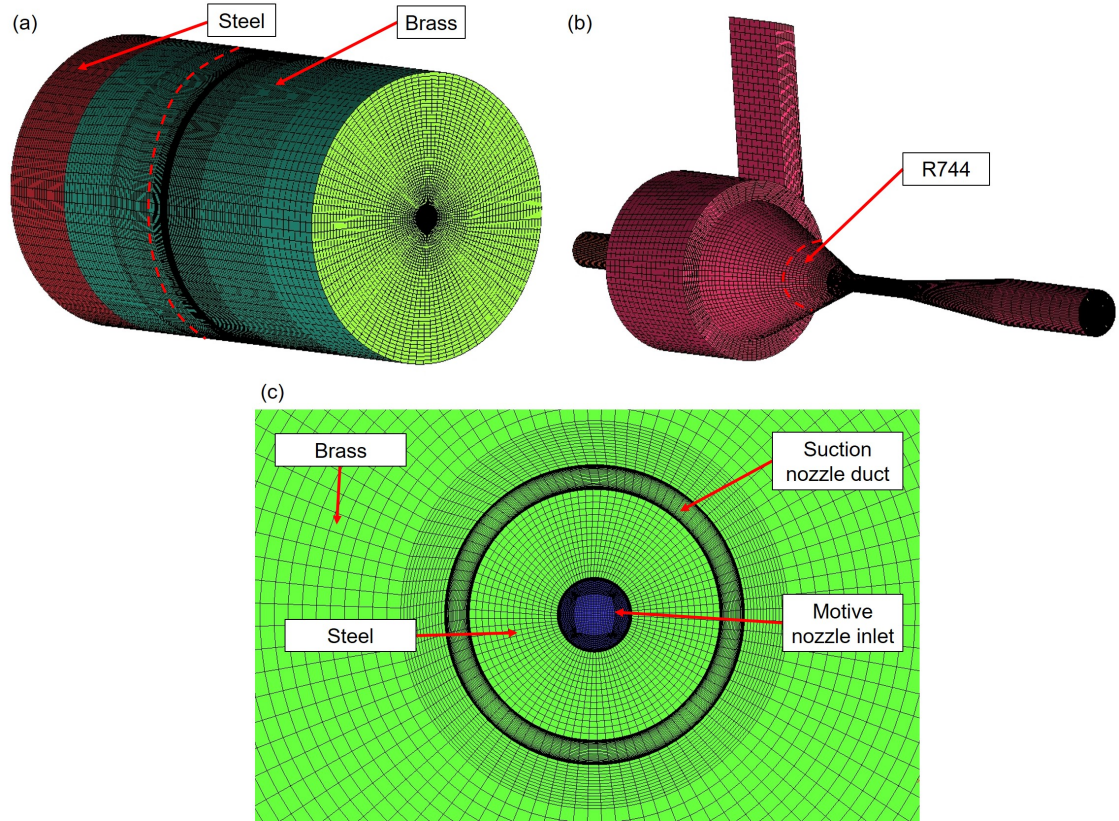
14

Figure 6: The numerical mesh grid of the R744 two-phase ejector: (a) outer solid walls; (b) interface between solid and fluid domains; (c) cross-sectional view through the motive nozzle throat.

Apart from the mesh sensitivity investigation, the grid convergence index (GCI) analysis was performed. The GCI analysis of χ was performed for the same boundary conditions #AD1 and numerical grids as for the aforementioned mesh sensitivity analysis presented in Figure 7 based on an approach defined by Roache et al. [43]. The grid refinement ratio r of 1.28 was constant during mesh refinement. The order of convergence was calculated as follows:

$$p_{GCI} = \frac{1}{ln\,(r)} |ln\left(|\frac{(\chi_c - \chi_m)}{(\chi_m - \chi_f)}|\right)| \tag{17}$$

where p_{GCI} is the order of convergence and subscripts c, m, and f are defined for coarse, medium, and fine meshes, respectively. To provide a weighted correction to the fine grid solution, a second-order Richardson extrapolation method can be used [44]:

$$\chi_{ext} = \chi_f + \frac{\chi_f - \chi_m}{r^2 - 1} \tag{18}$$

Finally, GCI of the fine mesh can be solved in the following form:

$$GCI_f = \frac{1.25 \cdot \frac{|\chi_f - \chi_m|}{\chi_f}}{r^p - 1} \tag{19}$$

where GCI_f is the fine-grid convergence index. The results of the GCI analysis were set in Table 6. The GCI value of 0.48% confirmed negligible influence of the selected numerical grid on the CFD results.
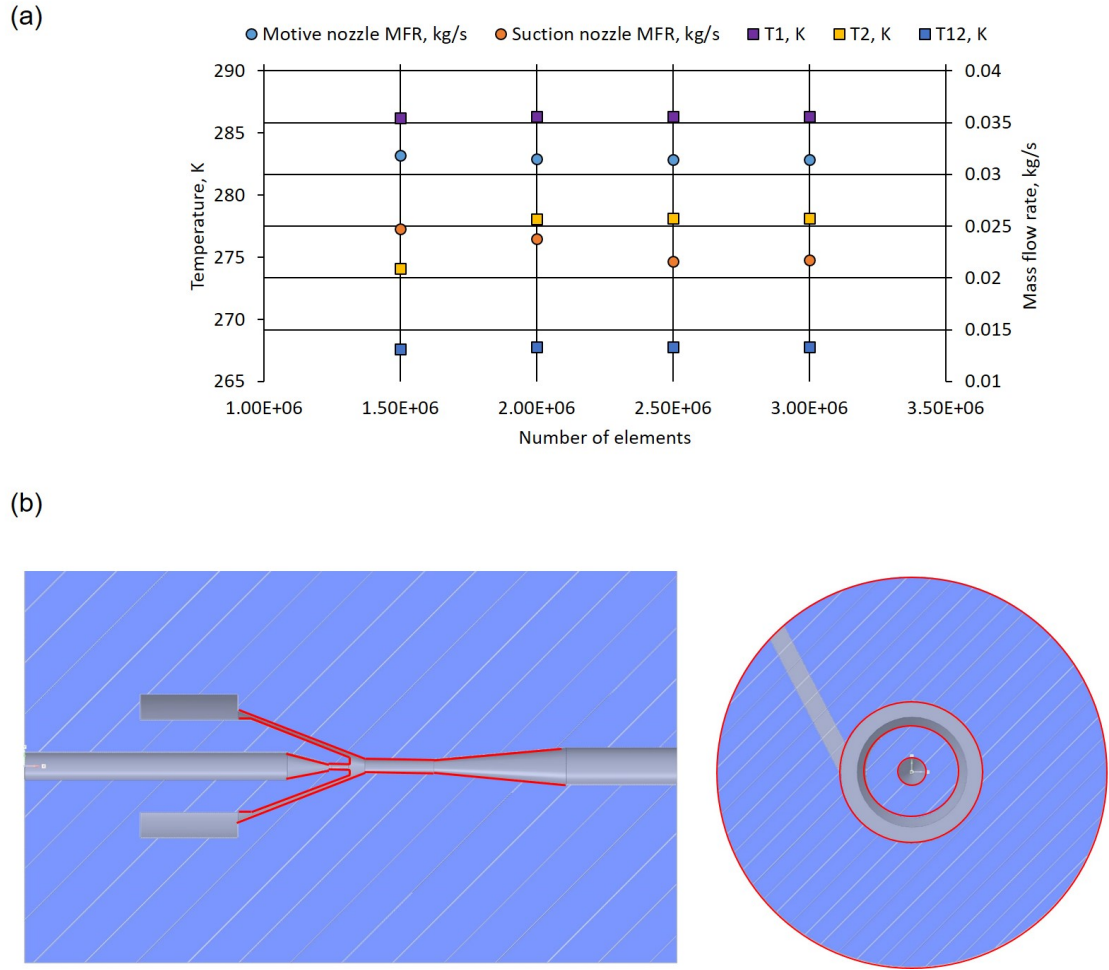
15

(a)

(b)

Figure 7: The mesh sensitivity analysis of the R744 two-phase ejector: (a) MN and SN MFRs and local wall temperatures at boundary conditions #AD1 defined in Table 4; (b) selected geometrical parameters for mesh refinement at the axial section and the cross-sections.

Table 6: Parameters of Grid convergence index analysis computed according to [43].

Parameter	Value
Constant grid refinement ratio (r)	1.28
Order of convergence (p_{GCI})	5.25
Extrapolated mass entrainment ratio (χ_{ext})	0.69
Fine-grid convergence index (GCI$_f$)	0.48%

The numerical investigation of the wall thermal conductivity and wall roughness influence on the wall temperature distribution was presented in Figure 8 for boundary condition #AD8 with high ΔT of approximately 28 K defined in Table 4. It can be seen that the change of the brass thermal conductivity negligible influenced the wall temperatures. An increase of k_w from 109 W/(m·K) to 153 W/(m·K) lowered wall temperature by 0.2 K at the measurement points as shown in Figure 8(a). The wall roughness sensitive analysis presented in Figure 8(b) indicated the walls temperature differences of the thermocouples 6÷13. The CFD model with wall roughness of 2 μm

16

obtained lower values of the foregoing wall temperatures up to approximately 6 K when compared to the results with higher wall roughness. Therefore, the wall roughness influenced the heat transfer inside the R744 ejector, thereby it should be taken into the account during the design process. The influence of different HTC defined on the outer ejector walls showed almost identical HTC on the inner walls temperature distribution was presented in Figure 8(c). In similar to the wall thermal conductivity, HTC defined on the outer ejector walls had negligible effect on the temperature distribution close to the inner walls. A change of HTC from 10 W/(m²·K) to 2 W/(m²·K) reduced the inner walls temperature of thermocouples 11÷13 up to 0.2 K. The negligible effect of different turbulence intensity on the inner wall temperature distribution was presented in Figure 8(d) for the motive nozzle inlet and Figure 8(e) for the suction nozzle inlet. The reduction of the motive nozzle turbulence intensity from 25% to 1% slightly decreased the inner wall temperatures in the motive nozzle part, mixer and at the beginning of the diffuser. The reverse behaviour of the turbulence intensity appeared in the suction nozzle inlet. The inner wall temperatures increased at the end of mixer and in the diffuser during decreasing of the turbulence intensity.
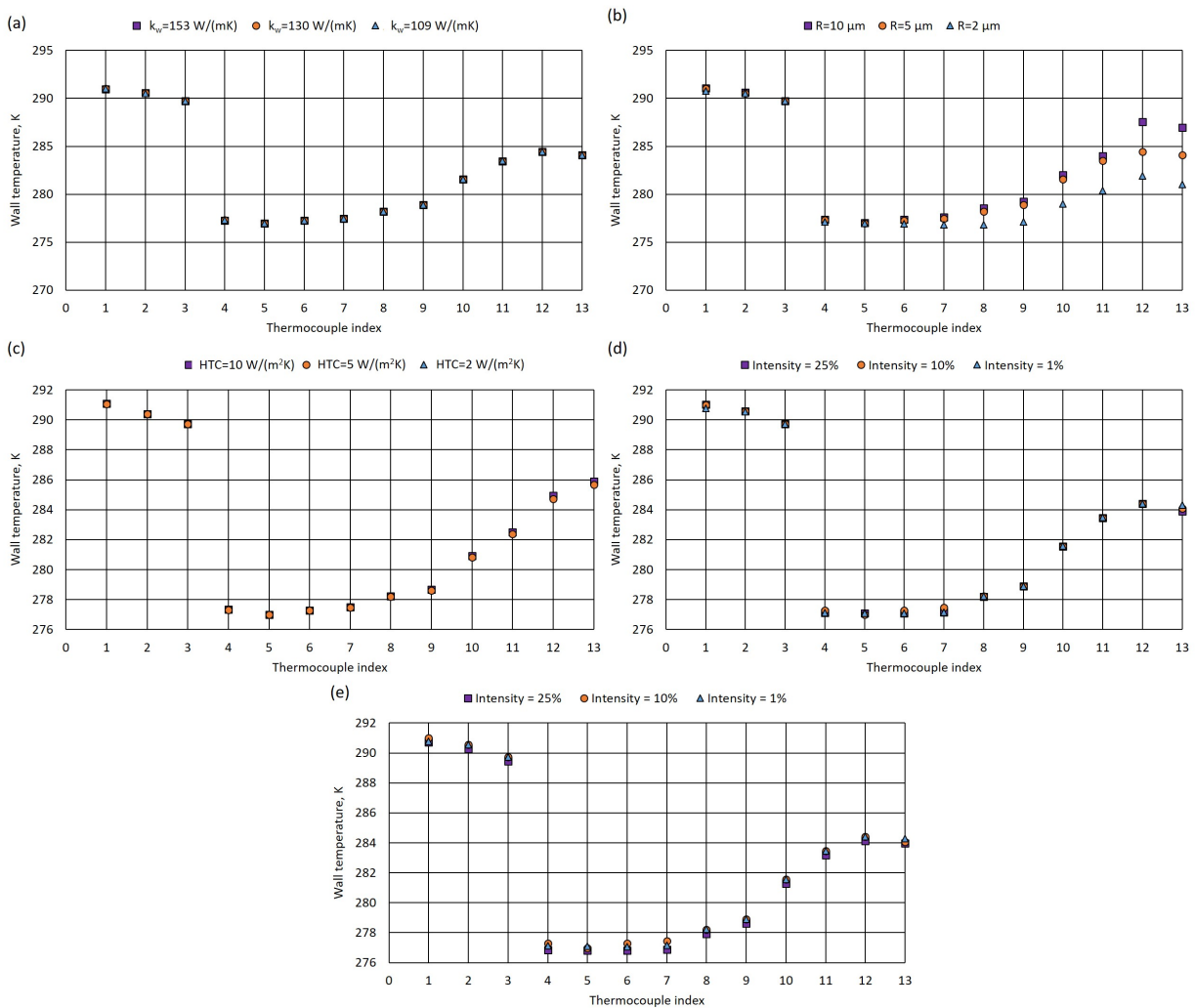

Figure 8: The sensitive analysis of the brass wall thermal conductivity and the wall roughness on the walls temperature distribution with boundary conditions #AD8 defined in Table 4:(a) the brass thermal conductivity; (b) wall roughness; (c) HTC defined on the outer ejector walls; (d) motive nozzle inlet turbulence intensity; (e) suction nozzle inlet turbulence intensity.

Figure 9 presents the influence of the turbulence model on the ejector walls temperature distribution and the ejector performance. The analysis was done for boundary condition #AD8 with high ΔT of 28 K defined in Table

17

4. The investigation was accomplished for four turbulence models: $k - \epsilon$ Realizable, $k - \omega$ SST, Transition SST and Reynolds Stress model and then the results were compared to the experimental data. Moreover, $k - \epsilon$ Realizable model and Reynolds Stress model required consideration of the near-wall treatment. In the aforementioned investigation, two near wall formulations were analysed:

- Standard wall function (SWT) that is used for a broad range of wall-bounded flows and it becomes less reliable, when the flow situations depart from the ideal conditions that are assumed in their derivation (30 < y$^+$ <300) [30].

- Enhanced wall function (EWT) that is used for complex near wall fluid phenomena or low-Reynolds flows (y$^+$ < 1) [30].

The $k - \omega$ SST, Transition SST and Reynolds Stress turbulence approaches took into account the near wall formulation in their mathematical structure. However, the low-Reynolds implementation was enabled for $k - \omega$ SST and Transition SST models to fully resolve the near wall boundary layer. The foregoing turbulence models were studied in the literature for the CFD numerical modelling of air and steam ejectors [28, 29, 30, 31]. As shown in Figure 9(a), the CFD model for each turbulence model obtained similar ejector walls temperatures for the thermocouples 1÷3. The temperature difference below 3 K was obtained for all investigated turbulence models for the thermocouples 4÷6 located close to the suction chamber and at the beginning of the pre-mixer. However, the mixing process of the motive and suction flows that appeared inside the pre-mixer and mixer strongly influenced the prediction of the wall temperatures. Hence, the $k - \epsilon$ Realizable SWT and $k - \omega$ SST approaches obtained high temperature difference for the thermocouples 8÷13 in the range from 10 K to 20 K.The better agreement of the near wall CO_2 fluid flow modelling in EWT affected the inner wall temperature prediction. Hence, the $k - \epsilon$ Realizable model with EWT reached a better prediction of the inner wall temperatures compared to the same turbulence approach with SWT, especially at the end of the diffuser. The best accuracy of the temperature captured in the mixer and diffuser walls was obtained for the Transition SST and Reynolds Stress turbulence models with either SWT or EWT function. Furthermore, the CFD model with Transition SST reached wall temperature differences of the thermocouples 12÷13 below 1 K. Besagni et al. [29] obtained similar overestimation of the thermal field for the $k - \epsilon$-based and $k - \omega$-based turbulence models compared to the experimental data near nozzle and in the centreline of an air ejector.

According to the χ comparison presented in Figure 9(b), the $k - \epsilon$ Realizable and Transition SST models obtained similar χ value when compared to the experimental results. The CFD model with $k - \omega$ SST and Reynolds Stress turbulence model reached lower χ of approximately 0.4. The slight difference of χ for each turbulence approach was obtained in the numerical study of Mazzelli et al. [28] and Besagni et al. [29]. Moreover, the results presented by Varga et al. [31] confirmed the best agreement of the global flow parameters by using the Transition SST approach. A use of the EWT in the $k - \epsilon$ Realizable and Reynolds Stress turbulence models increased χ compared to the aforementioned models with SWT. The similar behaviour was indicated in [30]. The best prediction of the wall temperature distribution and high accuracy of χ let to use the Transition SST turbulence model to the validation procedure and further investigations.

5.3. CFD model validation

Table 7 presents the motive nozzle and the suction nozzle MFR discrepancies together with the wall temperature discrepancies of the proposed R744 two-phase ejector CFD model with insulated outer walls. The validation procedure was performed for all boundary conditions presented in Table 4. It can be observed that the motive nozzle MFR prediction of the CFD model was within ±7%. The high accuracy of the motive nozzle MFR resulted in the low wall temperature discrepancy of thermocouples 1÷3 located in the motive nozzle below ±5 K. The suction nozzle MFR accuracy was within ±10% for all investigated points. The highest discrepancy of the suction nozzle MFR of 10.6% was obtained for #AD1. The wall temperature predictions above 5 K of the thermocouples 6÷11 located at the end of pre-mixer and in the mixer were reached for #AD5. However, the accuracy of the ejector wall temperatures was below 8 K for all boundary conditions of the thermocouples 4÷13. Therefore, the proposed CFD model of the R744 two-phase ejector with insulated outer walls predicted the motive nozzle and the suction nozzle MFRs together with the wall temperatures with acceptable accuracy.
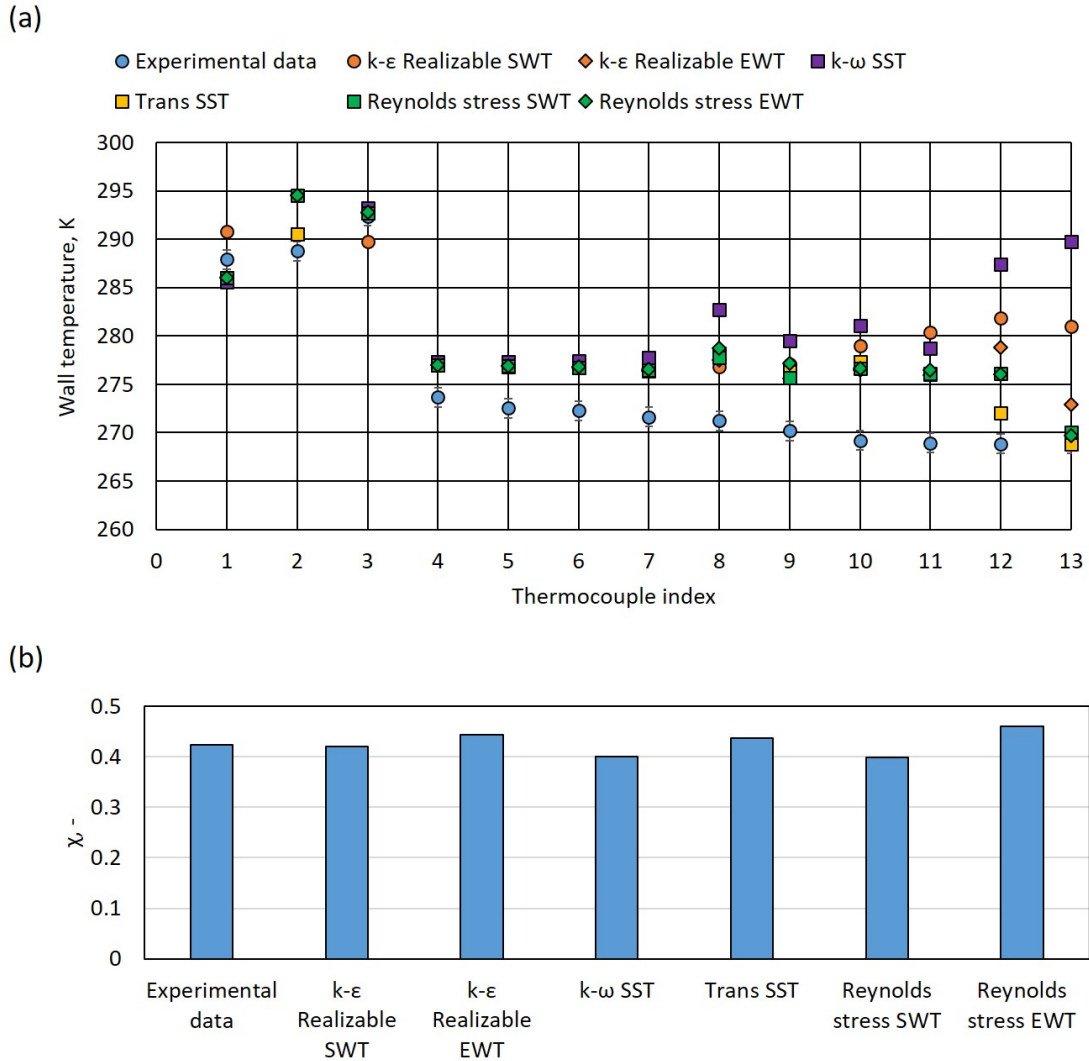
18

(a)

(b)

Figure 9: The turbulence model analysis of the R744 two-phase ejector with boundary conditions #AD8 defined in Table 4: (a) the wall temperature measurements; (b) χ value.

The validation procedure of the R744 two-phase ejector CFD model with non-adiabatic outer walls is presented in Table 8. Both nozzle MFRs and the wall temperatures predictions of the proposed CFD model were compared to the experimental data presented in Table 5. Similar to the results set in Table 7, the motive nozzle MFR accuracy was high: within ±5%. The suction nozzle MFR discrepancy was within ±10% for all boundary conditions except #NAD5. However, the suction nozzle MFR accuracy was below 12% for the foregoing boundary conditions, thereby the proposed CFD model predicted both streams at high accuracy at transcritical region and close to the critical point. The wall temperatures 1÷3 located in the motive nozzle part reached the absolute difference compared to the experimental data within ±3.0 K. The accuracy within ± 7 K was obtained for wall temperatures 4÷13 under boundary conditions #NAD1, #NAD2, #NAD4, #NAD6, and #NAD8, thereby the proposed CFD model predicted the wall temperature of the suction nozzle and the mixer with high accuracy. The highest discrepancy of the wall temperatures 9÷12 was within ±8 K at #NAD3, #NAD5 and #NAD7 as a result of the two-phase flow simulation within the mixer and the diffuser. However, the prediction of the wall temperatures 12 and 13 below ±5 K was reached for the remaining boundary conditions. Therefore, the proposed CFD model obtained

Table 7: The accuracy of the R744 two-phase ejector CFD model with AD outer walls.

BC	$\delta \dot{m}_{MN}$ %	$\delta \dot{m}_{SN}$ %	Δ_{T_1} K	Δ_{T_2} K	Δ_{T_3} K	Δ_{T_4} K	Δ_{T_5} K	Δ_{T_6} K	Δ_{T_7} K	Δ_{T_8} K	Δ_{T_9} K	$\Delta_{T_{10}}$ K	$\Delta_{T_{11}}$ K	$\Delta_{T_{12}}$ K	$\Delta_{T_{13}}$ K
#AD1	-5.4	10.6	1.8	2.0	0.4	1.9	2.4	2.6	3.8	3.3	4.4	3.9	2.0	-0.2	-0.2
#AD2	-5.1	0.2	3.5	2.2	0.3	-0.2	0.6	-0.4	-0.5	-0.3	0.2	0.7	0.7	-0.3	-0.5
#AD3	-1.9	7.9	0.5	-1.0	0.6	0.3	1.2	1.5	2.0	1.6	2.6	3.4	1.7	1.9	1.1
#AD4	-1.3	7.6	0.6	0.7	-1.9	3.5	4.3	4.4	7.9	5.5	7.6	5.8	3.4	1.4	-0.3
#AD5	-4.2	2.0	2.0	2.4	2.0	7.0	7.7	7.5	7.7	7.7	7.4	7.7	7.2	1.1	-0.3
#AD6	5.6	8.8	2.0	1.0	-0.8	1.2	1.9	2.0	2.3	2.7	3.4	3.5	4.5	4.0	3.7
#AD7	-7.2	6.5	4.3	2.6	0.3	2.9	3.3	3.4	3.6	3.6	4.5	5.4	5.7	4.9	0.6
#AD8	-0.7	5.6	-1.1	0.3	0.3	3.3	1.6	1.8	2.1	2.6	3.2	4.6	3.2	1.0	0.0

an accuracy range similar to that of the validation procedure presented in Table 7.

Table 8: The accuracy of the R744 two-phase ejector CFD model with NAD outer walls insulation.

BC	$\delta \dot{m}_{MN}$ %	$\delta \dot{m}_{SN}$ %	Δ_{T_1} K	Δ_{T_2} K	Δ_{T_3} K	Δ_{T_4} K	Δ_{T_5} K	Δ_{T_6} K	Δ_{T_7} K	Δ_{T_8} K	Δ_{T_9} K	$\Delta_{T_{10}}$ K	$\Delta_{T_{11}}$ K	$\Delta_{T_{12}}$ K	$\Delta_{T_{13}}$ K
#NAD1	-0.4	0.7	0.9	0.4	1.8	3.6	4.4	4.7	4.7	4.9	1.9	2.1	3.6	1.4	-0.6
#NAD2	-3.4	-5.8	-0.4	0.6	1.9	4.7	5.2	5.7	6.0	4.7	4.5	5.2	4.6	1.4	0.9
#NAD3	-2.7	-4.4	1.7	0.5	2.8	7.5	7.6	7.7	8.2	6.6	6.5	7.0	8.1	1.8	0.3
#NAD4	-2.9	-2.1	-0.7	0.7	1.3	4.3	5.0	5.4	5.7	3.6	3.8	5.5	4.2	0.3	-0.3
#NAD5	-0.7	11.0	1.5	0.8	2.9	5.8	6.3	6.3	6.6	6.1	6.3	7.4	7.9	4.1	0.5
#NAD6	-1.8	7.7	0.8	0.7	-1.4	2.9	3.8	4.2	4.4	0.8	1.7	4.5	6.1	0.8	-0.2
#NAD7	1.1	0.5	-0.7	-1.8	0.2	5.7	6.1	6.3	6.6	6.1	6.3	7.1	8.1	3.9	0.1
#NAD8	0.3	5.1	1.8	1.4	2.3	3.4	3.7	4.1	3.7	1.8	2.2	2.6	4.6	4.5	2.3

The validation procedure for both outer wall variants confirmed the high accuracy of the global and the local parameters of the proposed CFD model. Therefore, the numerical investigation of the non-adiabatic inner and outer walls enabled us to determine the influence of heat transfer within the ejector walls and of the two-phase flow on ejector performance.

5.4. Influence of heat transfer on ejector performance

Figure 10 presents the temperature field of the R744 two-phase ejector for the section A-A defined in Figure 2(a). The results are shown under the boundary condition #AD1, defined in Table 4. The investigation was accomplished for four different ejector wall temperature variants. In Figure 10(a), the inner and outer walls were adiabatic, whereby the temperature field only depended on the two-phase flow. The adiabatic outer walls and the non-adiabatic inner walls are presented in Figure 10(b). It can be observed that heat transfer between the motive flow and the inner wall of the motive nozzle influenced the temperature distribution, particularly in the converging-diverging nozzle. The distance between the two streams increased the suction stream temperature close to the inner wall. Therefore, the non-adiabatic inner wall and the material properties of the motive nozzle influenced the motive stream and the suction stream parameters as well as the two-phase mixing flow inside the

20

pre-mixer. In Figure 10(c), the motive nozzle inner walls were adiabatic, and the inner walls of the suction nozzle, the mixer and the diffuser together with the outer walls were defined as non-adiabatic walls. It can be observed that the insulation of the motive nozzle prevented the influence of heat transfer on the motive stream and the suction stream behaviour near the walls. Finally, the non-adiabatic inner and outer walls are shown in Figure 10(d). The temperature field was similar to the results presented for the adiabatic outer walls. Therefore, the ambient conditions did not influence the R744 two-phase ejector performance compared to the inner walls of the motive nozzle.
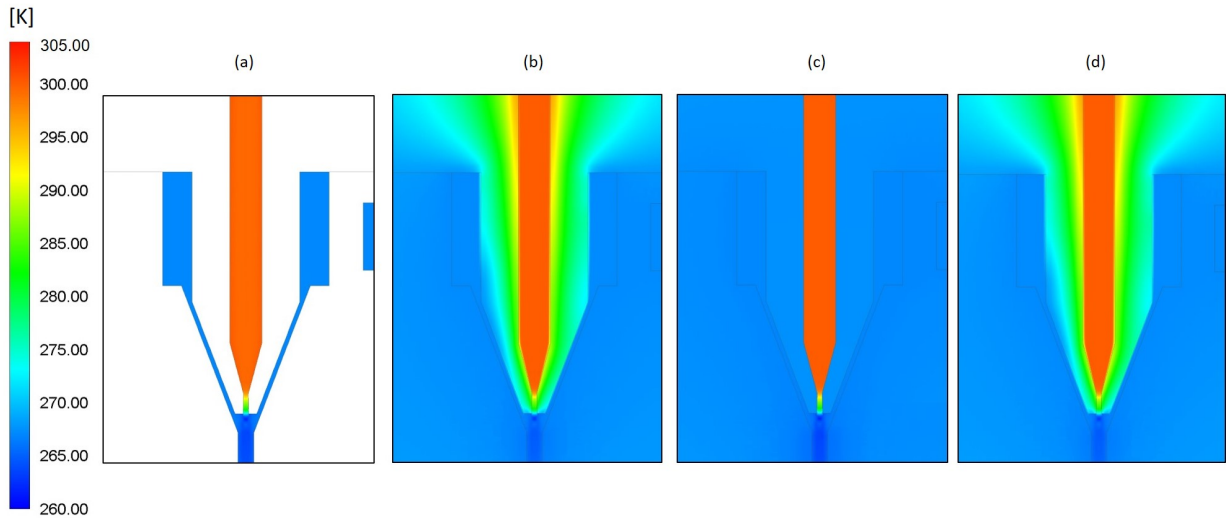
Figure 10: The temperature fields of the R744 two-phase ejector at boundary conditions #NAD2 defined in Table 5: (a) HT-1; (b) HT-2; (c) HT-3; (d) HT-4.

In addition to the temperature field presented in Figure 10, the investigation of the R744 two-phase suction flow behaviour enabled us to determine the influence of the tangential suction inlet on the flow swirl. Therefore, Figure 11 presents the streamlines of the R744 suction flow inside the two-phase ejector under boundary condition #NAD2 with high ΔT of approximately 26 K and the lowest suction pressure of 24.2 bar as defined in Table 5. The streamlines were coloured according to velocity magnitude to determine the region of the highest velocity. It can be observed that the suction flow formed a high swirl in the suction nozzle and in the mixer. As a result of the high rotational flow in the suction nozzle, the suction stream remained longer in the region near the motive nozzle inner wall. Therefore, the temperature increase of the swirled suction flow near the foregoing walls strongly influenced the mass flow rate and the performance of the two-phase ejector.

Figure 12 presents the influence of heat transfer on R744 two-phase ejector performance for four variants defined in Section 4.2. The investigation was performed for the two boundary conditions #AD1 and #AD4 defined in Table 4 and two boundary conditions #NAD6 and #NAD8 defined in Table 5. The foregoing boundary conditions were selected to analyse the heat transfer for different ΔT and different suction nozzle conditions. The motive nozzle MFR presented in Figure 12(a) confirmed the influence of heat transfer on the motive stream. The ejector with adiabatic inner walls in HT-1 exhibited lower MFR than the ejector with non-adiabatic inner walls in HT-2 and HT-4 under selected boundary conditions. In addition, the difference in the motive nozzle MFR between HT-2 and HT-4 was negligible. Considering the insulation of the motive nozzle inner walls in HT-3 was enough to enable us to determine a motive stream similar to that in HT-1.

The suction nozzle MFR analysis presented in Figure 12(b) enabled us to determine the influence of the suction stream temperature increase near the motive nozzle wall on the suction nozzle MFR value. The two-phase ejector with all adiabatic walls in HT-1 and adiabatic inner walls only in the motive nozzle exhibited higher suction nozzle MFR compared to the non-adiabatic inner walls in HT-2 and HT-4 under each boundary condition. The decrease in the suction nozzle MFR of approximately 0.1 kg/s under each boundary condition strongly influenced ejector performance. However, the insulation of the motive nozzle inner walls prevented the degradation of ejec-
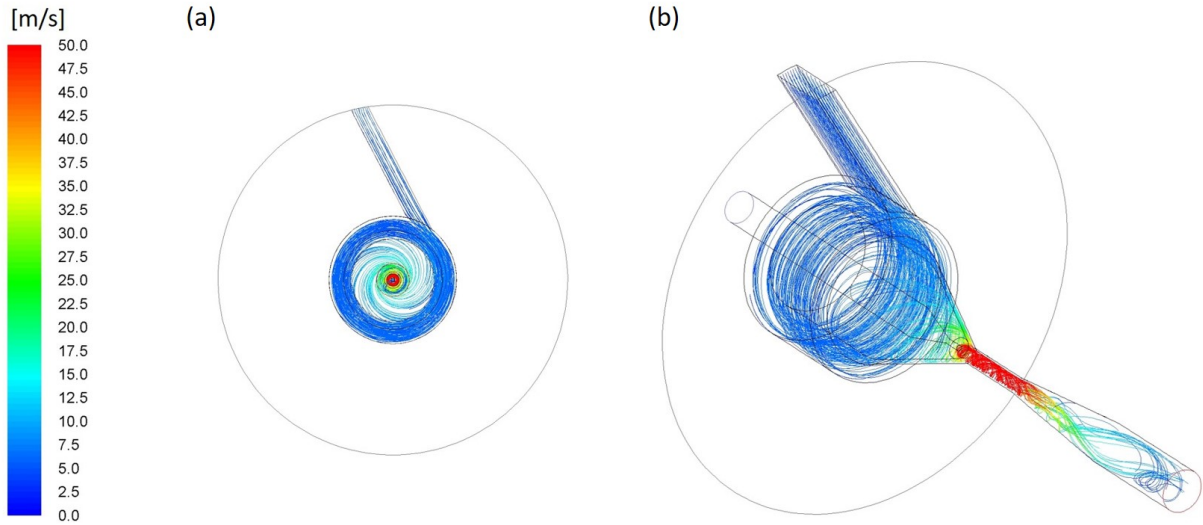
21

Figure 11: The suction flow streamlines coloured by the velocity magnitude of the R744 two-phase ejector at boundary conditions #NAD2 defined in Table 5:(a) cross-section view; (b) isometric view.

tor performance. Therefore, the effect of the swirling flow and the small thickness of the motive nozzle part close to the converging-diverging nozzle influenced the decrease in the suction nozzle MFR.

The increase in motive nozzle MFR and the decrease in suction nozzle MFR affected the decrease in χ, which was shown in Figure 12(c). The value of χ ranged from 0.42 to 0.6 aunder selected boundary conditions. However, the non-adiabatic inner walls in HT-2 and HT-4 decreased χ by approximately 0.1. In a manner similar to that described in the motive nozzle and suction nozzle MFR analysis, the two-phase ejector with adiabatic inner walls only in the motive nozzle achieved the best performance. Therefore, the highest relative degradation of χ for non-adiabatic walls (Figure 12(d)) was approximately 13% for HT-2 and HT-4 under #AD1. In addition, the ejector with non-adiabatic inner walls in HT-2 and HT-4 obtained a χ reduction over 10% under #AD4 and #NAD8. The lowest χ degradation of approximately 8% was reached under #NAD6 for HT-2 and HT-4. The two-phase ejector with adiabatic inner walls only in the motive nozzle defined in HT-3 obtained a small χ reduction below 1%. Therefore, an ejector should be constructed of low-conductivity material between the motive and suction nozzles. In addition, the replacement of the suction tangential inlet with an axial-type inlet improved ejector performance and reduced the influence of heat transfer between the nozzles.

5.5. Heat transfer coefficient of the R744 two-phase ejector

Figure 13 presents HTC of the CO_2 two-phase flow along the two-phase ejector for the motive nozzle, the mixer and diffuser. The HTC was investigated for boundary conditions #AD5 and #AD8 from Table 4 and #NAD1 and #NAD6 from Table 5. Similar to the results presented in Figure 12, the boundary conditions were selected for different ΔT from 8 K to 26 K. The highest HTC value of approximately 45 000 W/(m^{2}K) was obtained in the diverging part of the motive nozzle under #AD8 and #NAD1. Additionally, the HTC rapidly increased in the converging-diverging nozzle as a result of the expansion process, supersonic flow beyond the motive nozzle throat and the small distance between the two streams. The small thickness of the motive nozzle at the end of the diverging part influenced the high value of the heat flux and the temperature difference between the motive stream and the wall temperature (Figure 10). In the pre-mixer and the mixer, the HTC decreased below 5 000 W/(m^{2}K) as a result of the mixing process and the small impact of the brass wall temperature on heat transfer. Therefore, the R744 two-phase flow exhibited a similar HTC value in the mixer and in the diffuser. The high ΔT and the swirled suction flow affected the HTC increase in the diffuser (Figure 13) under #NAD6.

The HTC of the R744 suction flow inside the suction nozzle of the two-phase ejector is presented in Figure 14. The investigation was performed under boundary conditions #AD5, #AD8, #NAD1 and #NAD6 defined in
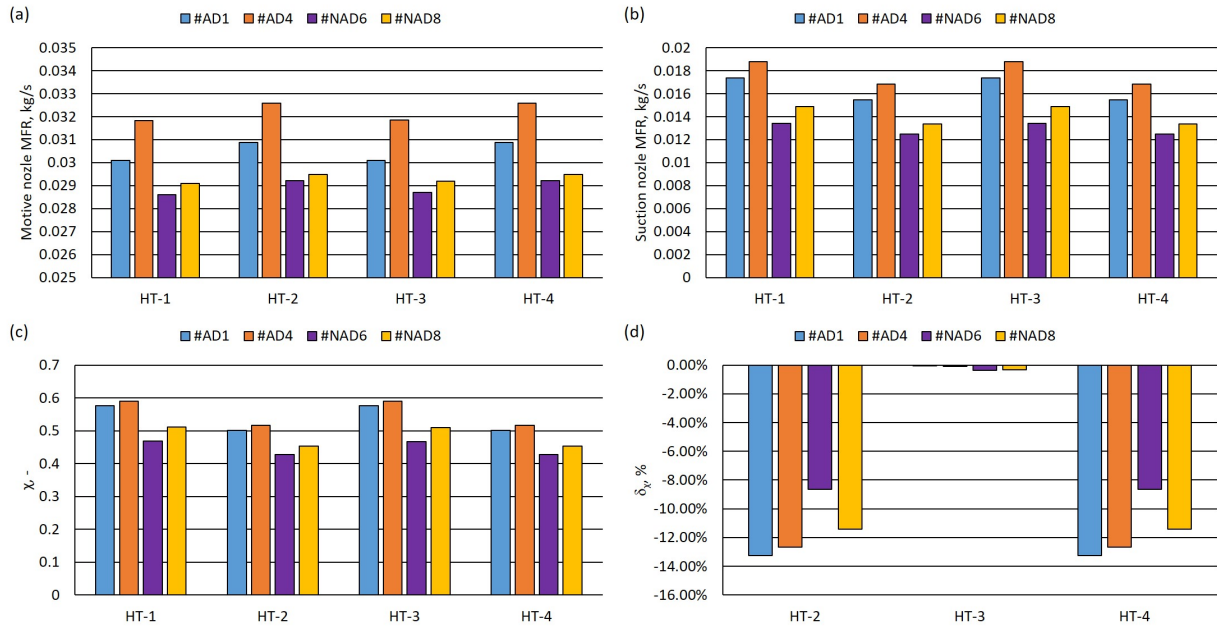
22

Figure 12: The heat transfer influence on the R744 two-phase ejector performance for four heat transfer variants at boundary conditions defined in Table 4 and Table 5: (a) motive nozzle MFR; (b) suction nozzle MFR; (c) mass entrainment ratio; (d) degradation of the mass entrainment ratio.
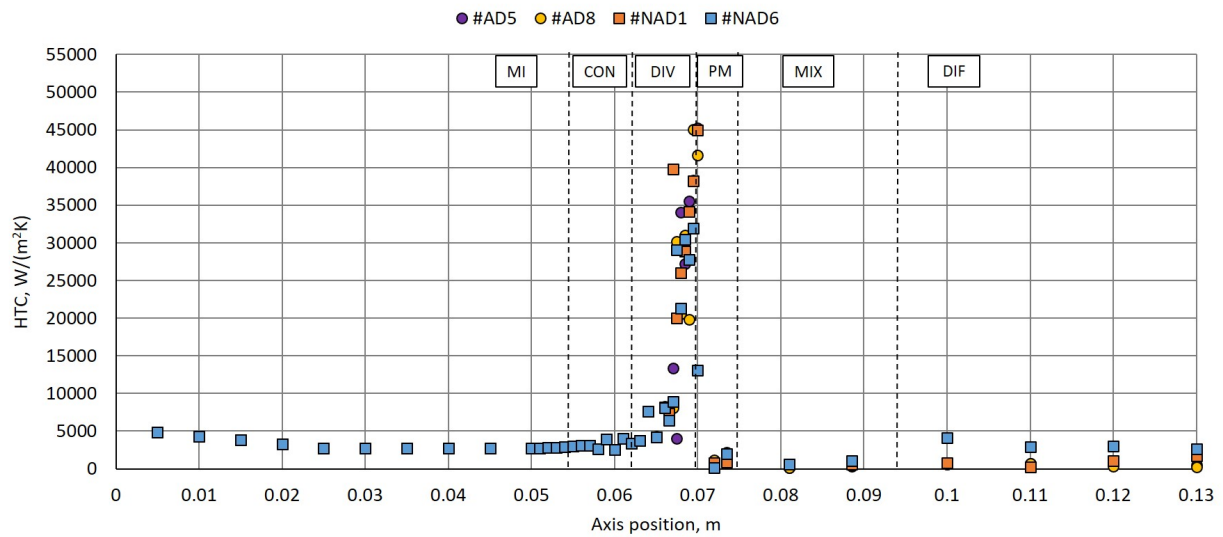

Figure 13: The HTC of the R744 two-phase flow along the two-phase ejector axis at boundary conditions defined in Table 4 and Table 5: MI - motive inlet; CON - motive nozzle converging part; DIV - motive nozzle diverging part; PM - pre-mixer; MIX - mixer; DIF - diffuser.

Table 4 and Table 5, respectively. In addition, the tangential inlet and the converging part of the suction nozzle were examined to evaluate the influence of the ejector design on the HTC calculations. The HTC value rapidly increased in the area of the tangential inlet and close to the pre-mixer. The highest HTC value of approximately $20\,000\ \mathrm{W/(m^2K)}$ was registered at the end of the tangential inlet under boundary condition #AD5. In addition, the swirled flow in the converging part of the suction nozzle slightly increased in response to the flow direction from approximately $100\ \mathrm{W/(m^2K)}$ to approximately $6\,000\ \mathrm{W/(m^2K)}$ for each investigated boundary condition. Finally,

the small distance between the motive stream and suction stream close to the pre-mixer influenced the high heat-flux values. Therefore, heat transfer strongly influenced the suction flow as a result of the suction inlet design and material selection.
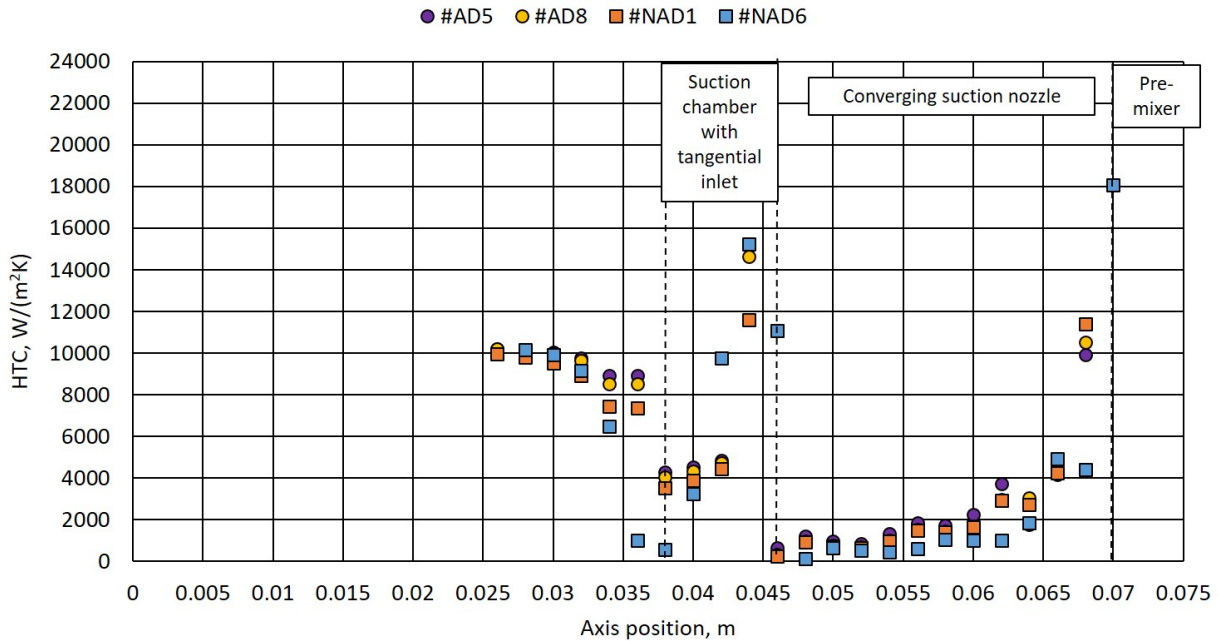
.

Figure 14: The HTC of the R744 two-phase flow inside the suction nozzle at boundary conditions defined in Table 4 and Table 5.

6. Conclusions

The proposed CFD model of the CO2 two-phase ejector was developed by coupling the heat transfer within the ejector walls with the two-phase HRM model. A R744 two-phase ejector equipped with thermocouples channels was designed and manufactured to perform an experimental investigation. A test series was performed on the two-phase ejector to evaluate ejector performance under the transcritical operating regime and near the critical point. The experimental investigation was performed with and without insulation of the outer ejector walls. In addition, the temperature difference between the motive nozzle and the suction nozzle was determined. The efficiency of the two-phase ejector ranged from 6% to 14% as a result of a small pressure difference between the outlet and the suction nozzle. In addition, the wall temperature distributions indicated the negligible influence of non-adiabatic outer ejector walls on the temperature along the ejector.

To determine the accuracy of the CFD model, the developed numerical model was verified and validated. A mesh sensitivity analysis was performed to avoid the influence of the numerical mesh grid on ejector performance. The Transition SST turbulence model was implemented to the CFD model regarding to the good prediction of the wall temperature distribution as well as the mass entrainment ratio when compared to the $k-\epsilon$ Realizable and $k-\omega$ SST models. The validation of the developed CFD model confirmed a good prediction of the mass flow rates. The motive nozzle MFR accuracy was within ±7% for ADs and NADs outer walls and the suction nozzle MFR accuracy was within ±10% for ADs and ±14% for NADs outer walls. Additionally, the wall temperature predictions of the two-phase R744 ejector CFD model were within ±5 K for most of the validated points. Therefore, the developed CFD model facilitated investigating the influence of heat transfer on ejector performance and calculating the HTC of the CO_2 two-phase flow.

24

The temperature field of the R744 two-phase ejector confirmed the negligible influence of ambient conditions on heat transfer within the ejector walls. However, non-adiabatic inner walls affected the fluid temperature distribution near the walls, particularly in the converging-diverging nozzle and the suction nozzle. In the suction nozzle, the tangential inlet caused a swirling flow of the suction stream, increasing the heat transfer process close to the inner walls. The non-adiabatic inner walls of the R744 two-phase ejector decreased the χ value from approximately 8% to 13%. The HTC along the motive nozzle and the suction nozzle confirmed the influence of heat transfer on the R744 two-phase flow, particularly in the converging-diverging nozzle, in the area of the tangential flow and close to the pre-mixer. Therefore, the use of low thermal conductivity materials may reduce the negative influence of heat transfer on ejector performance. However, to avoid device breakdown, the selection of the material from which to manufacture the ejector should also consider the stress on the motive nozzle caused by expansion.

7. Acknowledgement

References

[1] E. Parliament, C. of the European Union, Regulation (EU) no 517/2014 of the european parliament and of the council of 16 april 2014 on fluorinated greenhouse gases and repealing regulation (EC) no 842/2006 text with EEA relevance.

[2] M. H. Kim, J. Pettersen, C. W. Bullard, Fundamental process and system design issues in co2 vapor compression systems, Progress in Energy and Combustion Science 30 (2) (2004) 119–174. doi:10.1016/j.pecs.2003.09.002.
URL http://www.scopus.com/inward/record.url?eid=2-s2.0-1042288940&partnerID=40&md5=937deb77622c2dd30ccb15349ae081e3

[3] A. Hafner, S. Forsterling, K. Banasiak, Multi-ejector concept for r-744 supermarket refrigeration, International Journal of Refrigeration-Revue Internationale Du Froid 43 (2014) 1–13. doi:DOI10.1016/j.ijrefrig.2013.10.015.
URL <GotoISI>://WOS:000340979900002

[4] V. Sharma, B. Fricke, P. Bansal, Comparative analysis of various co2 configurations in supermarket refrigeration systems, International Journal of Refrigeration-Revue Internationale Du Froid 46 (2014) 86–99. doi:DOI10.1016/j.ijrefrig.2014.07.001.
URL <GotoISI>://WOS:000345233500011

[5] P. Gullo, K. Tsamos, A. Hafner, Y. Ge, S. A. Tassou, State-of-the-art technologies for transcritical r744 refrigeration systems – a theoretical assessment of energy advantages for european food retail industry, Energy Procedia 123 (2017) 46 – 53, proceedings of 1st International Conference on Sustainable Energy and Resource Use in Food Chains including Symposium on Heat Recovery and Efficient Conversion and Utilisation of Waste Heat ICSEF 2017, 19-20 April 2017, Windsor UK. doi:https://doi.org/10.1016/j.egypro.2017.07.283.

[6] S. Elbel, P. Hrnjak, Experimental validation of a prototype ejector designed to reduce throttling losses encountered in transcritical r744 system operation, International Journal of Refrigeration-Revue Internationale Du Froid 31 (3) (2008) 411–422. doi:DOI10.1016/j.ijrefrig.2007.07.013.
URL <GotoISI>://WOS:000254677900008

[7] S. Elbel, Historical and present developments of ejector refrigeration systems with emphasis on transcritical carbon dioxide air-conditioning applications, International Journal of Refrigeration-Revue Internationale Du Froid 34 (7) (2011) 1545–1561. doi:DOI10.1016/j.ijrefrig.2010.11.011.
URL <GotoISI>://WOS:000295752200002

[8] S. Minetto, R. Brignoli, K. Banasiak, A. Hafner, C. Zilio, Performance assessment of an off-the-shelf r744 heat pump equipped with an ejector, Applied Thermal Engineering 59 (1) (2013) 568 – 575. doi:https://doi.org/10.1016/j.applthermaleng.2013.06.032.

[9] J. S. Lee, M. S. Kim, M. S. Kim, Studies on the performance of a co2 air conditioning system using an ejector as an expansion device, International Journal of Refrigeration 38 (2014) 140 – 152. doi:https://doi.org/10.1016/j.ijrefrig.2013.08.019.

[10] Ángel Á. Pardiñas, A. Hafner, K. Banasiak, Novel integrated co2 vapour compression racks for supermarkets. thermodynamic analysis of possible system configurations and influence of operational conditions, Applied Thermal Engineering 131 (2018) 1008 – 1025. doi:https://doi.org/10.1016/j.applthermaleng.2017.12.015.

[11] G. Besagni, R. Mereu, F. Inzoli, Ejector refrigeration: A comprehensive review, Renewable and Sustainable Energy Reviews 53 (Supplement C) (2016) 373 – 407. doi:https://doi.org/10.1016/j.rser.2015.08.059.

[12] C. Lucas, H. Rusche, A. Schroeder, J. Koehler, Numerical investigation of a two-phase co2 ejector, International Journal of Refrigeration 43 (2014) 154–166. doi:http://dx.doi.org/10.1016/j.ijrefrig.2014.03.003.
URL http://www.sciencedirect.com/science/article/pii/S0140700714000504

[13] J. Smolka, Z. Bulinski, A. Fic, A. J. Nowak, K. Banasiak, A. Hafner, A computational model of a transcritical r744 ejector based on a homogeneous real fluid approach, Applied Mathematical Modelling 37 (3) (2013) 1208–1224. doi:http://dx.doi.org/10.1016/j.apm.2012.03.044.
URL http://www.sciencedirect.com/science/article/pii/S0307904X12002077

[14] F. Giacomelli, G. Biferi, F. Mazzelli, A. Milazzo, Cfd modeling of the supersonic condensation inside a steam ejector, Energy Procedia 101 (2016) 1224 – 1231, aTI 2016 - 71st Conference of the Italian Thermal Machines Engineering Association. doi:https://doi.org/10.1016/j.egypro.2016.11.137.
URL http://www.sciencedirect.com/science/article/pii/S1876610216313467

[15] E. W. Lemmon, M. L. Huber, M. O. McLinden, Nist standard reference database 23: Reference fluid thermodynamic and transport properties - refprop, National Institute of Standards and Technology, Standard Reference Data Program.

[16] M. Palacz, J. Smolka, A. Fic, Z. Bulinski, A. J. Nowak, K. Banasiak, A. Hafner, Application range of the hem approach for co2 expansion inside two-phase ejectors for supermarket refrigeration systems, International Journal of Refrigerationdoi:http://dx.doi.org/10.1016/j.ijrefrig.2015.07.006.
URL http://www.sciencedirect.com/science/article/pii/S0140700715002030

[17] M. Palacz, J. Smolka, A. J. Nowak, K. Banasiak, A. Hafner, Shape optimisation of a two-phase ejector for co2 refrigeration systems, International Journal of Refrigeration 74 (2017) 210–221. doi:http://dx.doi.org/10.1016/j.ijrefrig.2016.10.013.
URL http://www.sciencedirect.com/science/article/pii/S0140700716303425

[18] J. Bodys, M. Palacz, M. Haida, J. Smolka, A. J. Nowak, K. Banasiak, A. Hafner, Full-scale multi-ejector module for a carbon dioxide supermarket refrigeration system: Numerical study of performance evaluation, Energy Conversion and Management 138 (2017) 312 – 326. doi:http://dx.doi.org/10.1016/j.enconman.2017.02.007.
URL http://www.sciencedirect.com/science/article/pii/S019689041730105X

[19] K. Banasiak, A. Hafner, E. E. Kriezi, K. B. Madsen, M. Birkelund, K. Fredslund, R. Olsson, Development and performance mapping of a multi-ejector expansion work recovery pack for r744 vapour compression units, International Journal of Refrigeration 57 (2015) 265–276. doi:http://dx.doi.org/10.1016/j.ijrefrig.2015.05.016.
URL http://www.sciencedirect.com/science/article/pii/S0140700715001553

[20] M. Palacz, M. Haida, J. Smolka, A. J. Nowak, K. Banasiak, A. Hafner, Hem and hrm accuracy comparison for the simulation of co2 expansion in two-phase ejectors for supermarket refrigeration systems, Applied Thermal Engineeringdoi:http://dx.doi.org/10.1016/j.applthermaleng.2016.12.122.
URL http://www.sciencedirect.com/science/article/pii/S135943111634399X

[21] Z. Bilicki, J. Kestin, Physical aspects of the relaxation model in two-phase flow, Proceedings of the Royal Society of London A: Mathematical, Physical and Engineering Sciences 428 (1875) (1990) 379–397.
URL http://rspa.royalsocietypublishing.org/content/428/1875/379.abstract

[22] W. Angielczyk, Y. Bartosiewicz, D. Butrymowicz, J.-M. Seynhaeve, 1-d modeling of supersonic carbon dioxide two-phase flow through ejector motive nozzle, in: International Refrigeration and Air Conditioning Conference, 2362, Purdue University, Purdue ePubs, The address of the publisher, 2010, pp. 1–8, an optional note.
URL http://docs.lib.purdue.edu/iracc/1102

[23] M. Haida, J. Smolka, A. Hafner, M. Palacz, K. Banasiak, A. J. Nowak, Modified homogeneous relaxation model for the r744 trans-critical flow in a two-phase ejector, International Journal of Refrigerationdoi:https://doi.org/10.1016/j.ijrefrig.2017.10.010.
URL http://www.sciencedirect.com/science/article/pii/S0140700717303948

[24] M. Yazdani, A. A. Alahyari, T. D. Radcliff, Numerical modeling of two-phase supersonic ejectors for work-recovery applications, International Journal of Heat and Mass Transfer 55 (21–22) (2012) 5744–5753. doi:http://dx.doi.org/10.1016/j.ijheatmasstransfer.2012.05.071.
URL http://www.sciencedirect.com/science/article/pii/S0017931012003924

[25] Y. Liao, D. Lucas, 3d cfd simulation of flashing flows in a converging-diverging nozzle, Nuclear Engineering and Design 292 (2015) 149 – 163. doi:https://doi.org/10.1016/j.nucengdes.2015.06.015.
URL http://www.sciencedirect.com/science/article/pii/S0029549315002654

[26] Q. D. Le, R. Mereu, G. Besagni, V. Dossena, F. Inzoli, Computational fluid dynamics modeling of flashing flow in convergent-divergent nozzle, ASME: Journal of Fluids Engineeringn 140 (2018) 101102–1 – 101102–22. doi:http://dx.doi.org/10.1115/1.4039908.

[27] S. Croquer, S. Poncet, Z. Aidoun, Turbulence modeling of a single-phase r134a supersonic ejector. part 1: Numerical benchmark, International Journal of Refrigeration 61 (2016) 140 – 152. doi:https://doi.org/10.1016/j.ijrefrig.2015.07.030.
URL http://www.sciencedirect.com/science/article/pii/S0140700715002376

[28] F. Mazzelli, A. B. Little, S. Garimella, Y. Bartosiewicz, Computational and experimental analysis of supersonic air ejector: Turbulence modeling and assessment of 3d effects, International Journal of Heat and Fluid Flow 56 (2015) 305 – 316. doi:https://doi.org/10.1016/j.ijheatfluidflow.2015.08.003.
URL http://www.sciencedirect.com/science/article/pii/S0142727X15001101

[29] G. Besagni, R. Mereu, P. Chiesa, F. Inzoli, An integrated lumped parameter-cfd approach for off-design ejector performance evaluation, Energy Conversion and Management 105 (2015) 697 – 715. doi:https://doi.org/10.1016/j.enconman.2015.08.029.
URL http://www.sciencedirect.com/science/article/pii/S019689041500775X

[30] G. Besagni, F. Inzoli, Computational fluid-dynamics modeling of supersonic ejectors: Screening of turbulence modeling approaches, Applied Thermal Engineering 117 (2017) 122 – 144. doi:https://doi.org/10.1016/j.applthermaleng.2017.02.011.
URL http://www.sciencedirect.com/science/article/pii/S1359431116328290

[31] S. Varga, J. Soares, R. Lima, A. C. Oliveira, On the selection of a turbulence model for the simulation of steam ejectors using cfd, International Journal of Low-Carbon Technologies 12 (3) (2017) 233–243. arXiv:/oup/backfile/content_public/journal/ijlct/12/3/10.1093_ijlct_ctx007/1/ctx007.pdf, doi:10.1093/ijlct/ctx007.
URL http://dx.doi.org/10.1093/ijlct/ctx007

[32] D. V. Brezgin, K. E. Aronson, F. Mazzelli, A. Milazzo, The surface roughness effect on the performance of supersonic ejectors, Thermophysics and Aeromechanics 24 (9) (2016) 553–561. doi:http://dx.doi.org/10.1134/S0869864317040060.

[33] F. Mazzelli, A. Milazzo, Performance analysis of a supersonic ejector cycle working with r245fa, International Journal of Refrigeration 49 (2015) 79 – 92. doi:https://doi.org/10.1016/j.ijrefrig.2014.09.020.

26

[34] H. Zhang, L. Wang, L. Jia, H. Zhao, C. Wang, Influence investigation of friction on supersonic ejector performance, International Journal of Refrigeration 85 (2018) 229 – 239. doi:https://doi.org/10.1016/j.ijrefrig.2017.09.028.

[35] A. Milazzo, F. Mazzelli, Future perspectives in ejector refrigeration, Applied Thermal Engineering 121 (2017) 344 – 350. doi:https://doi.org/10.1016/j.applthermaleng.2017.04.088.

[36] J. Sinpiboon, S. Wongwises, Numerical investigation of refrigerant flow through non-adiabatic capillary tubes, Applied Thermal Engineering 22 (2002) 2015–2032.

[37] N. Agrawal, B. Souvik, Performance evaluation of a non-adiabatic capillary tube in a transcritical co_2 heat pump cycle, International Journal of Thermal Sciences 47 (2008) 423–430.

[38] K. Banasiak, M. Palacz, A. Hafner, Z. Buliński, J. Smołka, A. J. Nowak, A. Fic, A cfd-based investigation of the energy performance of two-phase r744 ejectors to recover the expansion work in refrigeration systems: An irreversibility analysis, International Journal of Refrigeration 40 (0) (2014) 328–337. doi:http://dx.doi.org/10.1016/j.ijrefrig.2013.12.002.
URL http://www.sciencedirect.com/science/article/pii/S0140700713003812

[39] K. Banasiak, A. Hafner, 1d computational model of a two-phase r744 ejector for expansion work recovery, International Journal of Thermal Sciences 50 (11) (2011) 2235–2247. doi:http://dx.doi.org/10.1016/j.ijthermalsci.2011.06.007.
URL http://www.sciencedirect.com/science/article/pii/S1290072911001876

[40] K. Banasiak, A. Hafner, T. Andresen, Experimental and numerical investigation of the influence of the two-phase ejector geometry on the performance of the r744 heat pump, International Journal of Refrigeration 35 (6) (2012) 1617–1625. doi:http://dx.doi.org/10.1016/j.ijrefrig.2012.04.012.
URL http://www.sciencedirect.com/science/article/pii/S014070071200093X

[41] M. Haida, J. Smolka, A. Hafner, Z. Ostrowski, M. Palacz, K. B. Madsen, S. Försterling, A. J. Nowak, K. Banasiak, Performance mapping of the r744 ejectors for refrigeration and air conditioning supermarket application: A hybrid reduced-order model, Energy 153 (2018) 933 – 948.

[42] A. Fluent, Ansys fluent user's guide, PA, Canonsburg.

[43] P. J. Roache, Perspective: A method for uniform reporting of grid refinement studies, ASME Journal of Fluids Engineering 116 (3) (1994) 405 –413. doi:http://dx.doi.org/10.1115/1.2910291.

[44] C. J. Freitas, The issue of numerical uncertainty, Applied Mathematical Modelling 26 (2) (2002) 237 – 248. doi:https://doi.org/10.1016/S0307-904X(01)00058-0.
URL http://www.sciencedirect.com/science/article/pii/S0307904X01000580